INVESTIGATION OF DIAMOND COATINGS ON IRON BASED MATERIALS BY

MICROWAVE PLASMA CHEMICAL VAPOR DEPOSITION

A Thesis Submitted to the College of

Graduate Studies and Research

In Partial Fulfillment of the Requirements

For the Degree of Master of Science

In the Department of Mechanical Engineering

University of Saskatchewan

Saskatoon

By

Xiaoyu Sun

PERMISSION TO USE

In presenting this thesis in partial fulfilment of the requirements for a Postgraduate degree from the University of Saskatchewan, I agree that the Libraries of this University may make it freely available for inspection. I further agree that permission for copying of this thesis in any manner, in whole or in part, for scholarly purposes may be granted by Professor Q. Yang who supervised my thesis work or, in their absence, by the Head of the Department or the Dean of the College in which my thesis work was done. It is understood that any copying or publication or use of this thesis or parts thereof for financial gain shall not be allowed without my written permission. It is also understood that due recognition shall be given to me and to the University of Saskatchewan in any scholarly use which may be made of any material in my thesis.

Requests for permission to copy or to make other use of material in this thesis in whole or part should be addressed to:

Head of the Department of Mechanical Engineering

University of Saskatchewan

57 Campus Drive

Saskatoon, Saskatchewan S7N 5A9

Canada

ABSTRACT

Diamond thin films on Fe based materials (ferrous alloys) for the purpose of improving their surface properties such as wear and corrosion resistance have been investigated. There are main barriers restricting the quality and adhesion of diamond coatings on Fe based materials. Firstly, the incubation time of diamond nucleation is long due to the high solubility of carbon in Fe. Secondly, graphite soot forms before diamond nucleation due to the catalytic effect of Fe for formation of graphitic carbon. Thirdly, high internal stress remains at the interface which is induced by the large difference in the thermal expansion coefficients of diamond and most of the Fe based materials. Surface modification and interlayers are two important approaches to overcome these problems. In this work, the effect of Cr content in Fe-Cr alloys on diamond nucleation and growth is being studied in order to clarify the mechanisms of Cr in diamond deposition. Furthermore, in order to enhance the adhesion and quality of diamond coatings, Al based interlayers are being investigated on ferrous alloys.

Fe-Cr alloys (with 20~80 wt.% Cr) were exposed to a CH_4-H_2 mixture in a microwave plasma enhanced chemical vapor deposition (MPCVD) reactor. Severe metal dusting and carburization were observed on the alloys with low Cr content and diamond did not nucleate on those alloys until a graphite intermediate layer had been formed, which takes a long incubation time. Increasing Cr concentration in the Fe-Cr alloys promotes the formation of a Cr carbide buffer layer, which inhibits metal dusting and the formation of graphite soot. Consequently, diamond nucleation and growth can be greatly enhanced, and continuous diamond films with enhanced adhesion have been deposited on the Fe-80Cr alloys.

Al based interlayers including Al and Al/AlN interlayers were deposited on ferrous alloys (SS316 and Kovar: FeNiCo) to enhance diamond deposition. The deposition was carried out in a microwave plasma chemical vapor deposition (MPCVD) reactor using a CH_4-H_2 mixture. The

obtained samples were characterized using X-ray diffraction (XRD), scanning electron microscopy (SEM), Raman spectroscopy, synchrotron-based X-ray absorption spectroscopy (XAS) and indentation testing. The results show that a single Al layer can effectively suppress the formation of graphite at the interface and the inward diffusion of carbon into Fe based substrates, and thereby enhances diamond nucleation and growth. The dual layers of Al/AlN can further enhance the adhesion of diamond coatings comparing with the single Al interlayer.

ACKNOWLEDGMENTS

DEDICATION

To my parents Sun, Jiabing and Deng, Li.

TABLE OF CONTENTS

LIST OF TABLES

LIST OF FIGURES

LIST OF ABBREVIATIONS

<u>Abbreviation</u>

AISI	American Iron and Steel Institute
BF	Bright field
BSE	Backscattered electron
BTIBD	Biased target ion beam deposition
c-AlN	Zincblend phase AlN
CLS	Canadian Light Source
CRT	Cathode ray tube
CTE	Coefficients of thermal expansion
CTEM	Conventional transmission electron microscopy
CVD	Chemical vapor deposition
DPD	Diamond particle density
EDS	Energy-dispersive X-ray spectroscopy
EH	End-Hall
EXAFS	Extended X-ray absorption fine structure
fcc	face-centered cubic
FEG	Field emission gun
FET	Field-effect transistor
FWHM	Full width at half maximum
FY	Fluorescent yield
h-AlN	Wurtzite phase AlN
HFCVD	Hot filament chemical vapor deposition

HPHT	High pressure high temperature
HVOF	High velocity oxy-fuel spraying
IBD	Ion beam deposition
Kovar	FeNiCo alloy
MEMS	Micro-electro-mechanical systems
MPCVD	Microwave plasma enhanced chemical vapor deposition
NSD	Nanostructured diamond
PVD	Physical vapor deposition
RF	Radio frequency
SE	Secondary electron
SEM	Scanning electron microscopy
SGM	Spherical grating monochromator
SS	Stainless steel
STEM	Scanning transmission electron microscopy
TEM	Transmission electron microscopy
TEY	Total electron yield
WDS	Wavelength-dispersive X-ray spectroscopy
XANES	X-ray absorption near edge structure
XAS	X-ray absorption spectroscopy
XRD	X-ray diffraction

CHAPTER 1
INTRODUCTION

1.1   Research Motivations

Synthetic diamond has attracted great attention owing to its advantageous properties, such as high hardness, high thermal conductivity, low friction coefficient, high corrosion resistance, optical transparency, chemical inertness, biocompatibility, and etc. Diamond coatings are promising for many applications in various industries, such as mechanical, optical, thermal, electrical, and biomedical fields [1–4].

Diamond films are deposited on Fe based materials to improve their surface properties, such as hardness, corrosion resistance and wear resistance. Stainless steel grade 316 (SS316) has been widely used for marine and biomedical applications due to its high strength, high corrosion resistance, and good biocompatibility [5]. However, its relatively low hardness and low abrasive wear resistance restrict many of its applications. Diamond coating can significantly improve hardness and wear resistance of SS316 and thus the coated materials could meet the requirements for broader applications. FeNiCo alloy (Kovar) is a good candidate material suitable for electrical devices and glass seals due to its low thermal expansion coefficient. Diamond coatings show similar low thermal expansion coefficient but much higher hardness and thermal conductivity than Kovar. It would be very promising to employ diamond coatings on Kovar to improve its thermal conductivity and wear resistance. The functional and protective properties of diamond coatings could prolong the lifetime and enhance the performance of products made of Fe based materials. Therefore, the deposition of diamond coatings on Fe based materials is of strategic importance.

Nevertheless, it is difficult to synthesize high quality and well adherent diamond coatings on Fe base substrates. One main barrier is the long incubation time of diamond nucleation due to

the high solubility of carbon into Fe based substrates. Secondly, the formation of graphite soot takes place on the surface of the substrates before diamond nucleation due to the catalytic effect of Fe for the formation of graphitic carbon. Finally, high interfacial stress would be induced by the large difference in thermal expansion coefficients of diamond and most of the Fe based materials. The high stress leads to a delamination or poor adhesion of diamond coatings [1,6–9].

Researchers have made efforts to overcome these technological problems in many ways. These include deposition process optimization, substrate modification, and applying interlayers. Nitriding, boriding, and alloying were used for surface modification [10–13]. These methods partially enhance the nucleation and growth of diamond coatings due to the formation of nitride, boride and alloy phases on the surface of the substrates. Various intermediate interlayers were also applied to eliminate the catalytic effect of Fe, such as metallic interlayers of W, Cr, Ti, Zr, Al, Mo, ceramic interlayers of CrN, AlN, TiN, and multi-interlayers of W/Al and TiC/Ti(C,N)/TiN [14–22]. These interlayers have significantly enhanced the quality and adhesion of diamond coatings. However, the enhancement of adhesion has been very limited. In order to meet the requirements of industrial applications, well adherent and high purity diamond coatings are needed. Optimization of the interlayers is one of the main solutions to achieve the goal. Researchers are investigating interlayers in many aspects, including the materials selection and structures design. However, the failure potential is high as interlayers create multi interfaces. Surface modification is an important alternative approach as it only results in single interface.

Both Cr and Al have beneficial effects on diamond nucleation and growth. The effect of Cr in ferrous alloys with a low fraction (<20 wt.%) of Cr has been studied, and the results show that Cr has little effect on diamond nucleation and growth [12,23]. Using Cr as interlayer was reported to be successful in improving the adhesion of diamond film on steels [15,24,25],

2

primarily attributed to the formation of chromium carbides. On the other hand, the adhesion failure of diamond coating was observed on Cr interlayers due to the large residual stress [26]. As a result, the underneath mechanism and the critical content of Cr to enhance diamond deposition need to be investigated. It has been reported that Al is a more effective alloying element for improvement of diamond nucleation and growth comparing to other alloying elements such as Ti, Cr, Si, and Mo [12]. Continuous and adherent diamond coatings have been deposited on steels with Al or AlN interlayer [17,20,22], in which the interlayers successfully suppressed the formation of graphite and the diffusion of carbon into substrates. Moreover, the interlayers can increase the nucleation density of diamond. However, a single layer of Al cannot eliminate the large thermal stress within the diamond coatings. Besides that, Al layer is soft and easily removed during the pre-scratch treatment. AlN has a lower thermal expansion coefficient than Al, which is expected to reduce the residual stress of diamond coatings. In addition, the hardness of AlN is higher than Al, which could prevent the failure of Al layer during pre-treatment process. Double-interlayers are thus developed in order to combine the advantageous properties of Al and AlN layers.

1.2   Research Objectives

The overall objective of this thesis is to obtain well adherent and high purity diamond coatings on iron based materials by alloying modification of substrates and addition of interlayers. Specifically, the research has following objectives:

1.   Evaluating the effect of Cr content in Fe-Cr alloys on diamond nucleation and growth.

2.   Synthesis of well adherent diamond coatings on Fe-Cr alloys using microwave plasma enhanced chemical vapor deposition (MPCVD).

3.   Synthesis of well adherent diamond coatings on commercial alloys: SS316 and Kovar by employing appropriate interlayers.

4.   Understanding the enhancement mechanisms of interlayers on diamond nucleation and deposition onto SS316 and Kovar substrates.

1.3   Methodology

Synthesis of diamond was conducted in a microwave plasma enhanced chemical vapor deposition (MPCVD) reactor. Interlayers were prepared using a biased target ion beam deposition (BTIBD) system. The morphology was observed by using optical microscopy, scanning electron microscopy (SEM), and transmission electron microscopy (TEM). The structural characteristics of the carbon coatings were characterized by Raman spectroscopy, X-ray diffraction (XRD), and Energy-dispersive X-ray spectroscopy (EDS). The structure of the interlayers was characterized using X-ray absorption near edge structure (XANES). The adhesion of the diamond coatings was evaluated using Rockwell C indentation testing.

1.4   Thesis Organization

This thesis is comprised of five chapters. Chapter 1 generally introduces the motivation, objective, methodology and organization of the thesis. Chapter 2 reviews the literatures in the research field, including the fundamentals, the synthesis techniques, the characterization techniques, and the research progress of diamond deposition on Fe based substrates. Chapter 3 gives the experimental details of the research work, including the deposition of diamond coatings on bare Fe-Cr substrates and interlayered commercial alloys. Chapter 4 presents the results and discussion of the research work correspondingly. Chapter 5 summarizes and concludes the research and thus suggests some future work.

CHAPTER 2
LITERATURE REVIEW

2.1   Diamond Coatings

2.1.1   Structure of Carbon Allotropes

Natural diamond has a specific face-centered cubic (fcc) crystalline structure, which is called diamond lattice. As shown in Fig. 2-1a, each plane in the diamond lattice consists of a 6-atom hexagonal ring arrangement. The bonding length of the adjacent atoms is 1.54 Å and the lattice constant is 3.56 Å. As shown in Fig. 2-1b, the carbon atoms have the most concentrated form of tetrahedral configuration. Each carbon atom shares all available electrons with four adjacent atoms and exhibits an sp^3 hybridization [4,27–29]. This type of covalent bonding provides diamond the strongest chemical linkage as known, which leads to many advantageous properties of diamond.
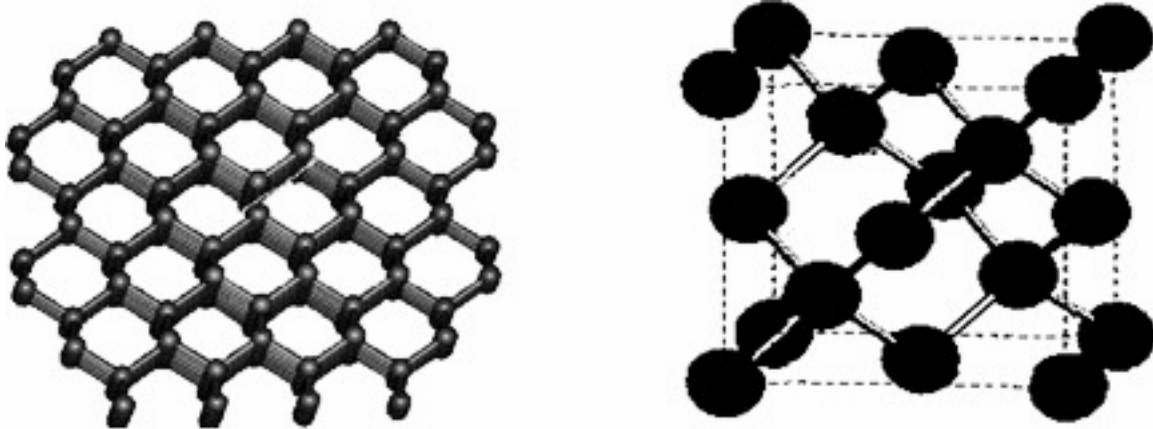
Figure 2-1. Diamond lattice (a) and a unit cell of diamond crystalline structure (b) [29].

Graphite is the most common form of carbon and has a hexagonal structure. The atoms are bonded as a hexagonal ring in a flat plane, while the rings in diamond are alternately dislocated. The lattice constant of graphite is 6.707 Å for c and 1.47 Å for a. Diamond synthesized by chemical vapor deposition is polycrystalline and contains primarily sp^3 bonding

5

in the grains, and sp^2 bonding at the grain boundaries. Amorphous carbon has also been synthesized by vapor deposition, which consists of a mixture of both sp^3 bonding and sp^2 bonding. In the past decades, many carbon nanomaterial with various structures have been synthesized and studied, such as diamond like carbon, fullerene, carbon nanotubes, graphene etc. [30–39].

2.1.2 Properties and Applications of Diamond Coatings

The unique structure of diamond contributes to its unique properties. Because of the strong covalent bonding and short bonding distance, diamond has high hardness and wear-resistance and is chemical inert and corrosion resistant. The carbon atoms in diamond lattice have high vibration frequency due to their low mass and high restoring force. As a result, the thermal conductivity of diamond is higher than most known materials at room temperature. Another notable property of diamond is the large bandgap (5.5 eV), which makes it a good insulator at room temperature and a wide range of transparency from ultraviolet to infrared radiation. High breakdown field or high frequency photons are needed to excite the electrons to conduction band. Also, it is shown that diamond has a negative electron affinity, which allows it to emit electrons easily when electric field is applied [1,28,40].

Diamond coatings have a wide range of potential applications in mechanical, biomedical, chemical, electrical and optical fields, such as insert [41,42], end-mill [43], biosensor [3], micro-electro-mechanical systems (MEMS) [2], field-effect transistor (FET) devices [44], optical fibres [45], and etc. Diamond-coated materials can combine both the properties of the substrates and diamond coatings to meet the demands of advanced technology.

6

2.2 Synthesis of Diamond Coatings

2.2.1 Chemical Vapor Deposition

Synthesis of diamond was firstly reported by General Electric in 1955 [46] using high pressure high temperature (HPHT) method under equilibrium conditions to convert graphite to diamond [47]. In this approach, graphite was compressed in high pressure about 80–100 kbar and heated to temperature up to 2800 °C. After that, catalysts were developed to reduce the conversion energy of graphite to diamond at relatively low pressure and low temperature. HPHT was suitable to produce single crystals of diamond from nanometer to millimeter scale. The applications of diamond synthesized by this method were restricted because of the high cost of the synthesis equipment and the high energy consumption during HPHT processing.

Since 1958, researchers have been trying to develop methods to synthesis diamond by decomposition of carbon-containing gases, which is known as chemical vapor deposition (CVD) [48–50]. The tetrahedral bonded carbon was produced by adding single carbon atom at one time to the existing template. CVD process could be carried out at low pressure and temperature lower than 1000 °C. The equipment and energy cost of CVD is lower compared to HPHT. Moreover, unlike HPHT, CVD is suitable for synthesis of diamond thin films with large area for various applications. Extensive studies on CVD diamond have been carried out. In 1982, Matsumoto et al. built a hot filament reactor to activate the precursor containing hydrogen and hydrocarbon gases [51]. This approach significantly improved the quality and growth rate of diamond films. Thereafter, various CVD methods have been developed and investigated to synthesize diamond thin films. The CVD process could be assisted by direct current plasma [52], radio frequency (RF) plasma [53], combustion flame [54], direct current plasma jet [55], microwave plasma [56], electron cyclotron resonance microwave plasma [57], or their modifications. Hot filament chemical vapor deposition (HFCVD) and microwave plasma chemical vapor deposition

(MPCVD) are the most popular CVD techniques for diamond synthesis. HFCVD has advantages of low cost and simplicity. As hot filaments are used, such as W, Ta and Re, the diamond coatings are easily contaminated by the evaporation of the metal filaments. The generation of plasma in MPCVD eliminates the requirement of electrode. Also, the plasma is enclosed above the substrate so that the deposition rate on chamber is slow. Overall, MPCVD has advantages of high quality deposition and stability comparing to other CVD techniques. The limitation of MPCVD is the difficulty to achieve high speed and large-scale deposition.

A typical schematic of MPCVD system is shown in Fig. 2-2. A microwave generator is installed above the chamber. An electric discharge is created by the microwave power through a quartz window. A waveguide is used to convert and direct the microwave from rectangular to circular. The microwave energy (frequency of 2.45 GHz) oscillates the gas phase electrons. High rate ionization takes place due to the collisions of the gas. The microwave plasma contains electrons, ions and neutrals dissociated from the gas molecules. The "hot" electrons have high energy as hundreds of eV, while the ions are "cool" at room temperature. The plasma ball is stable and adjustable by tuning the waveguide. The position of the plasma ball is dependent on the power, working pressure, and precursor composition. The substrates are mounted on a metal stage underneath the plasma. The deposition is performed as the surface of substrates immersed in the plasma ball [58].
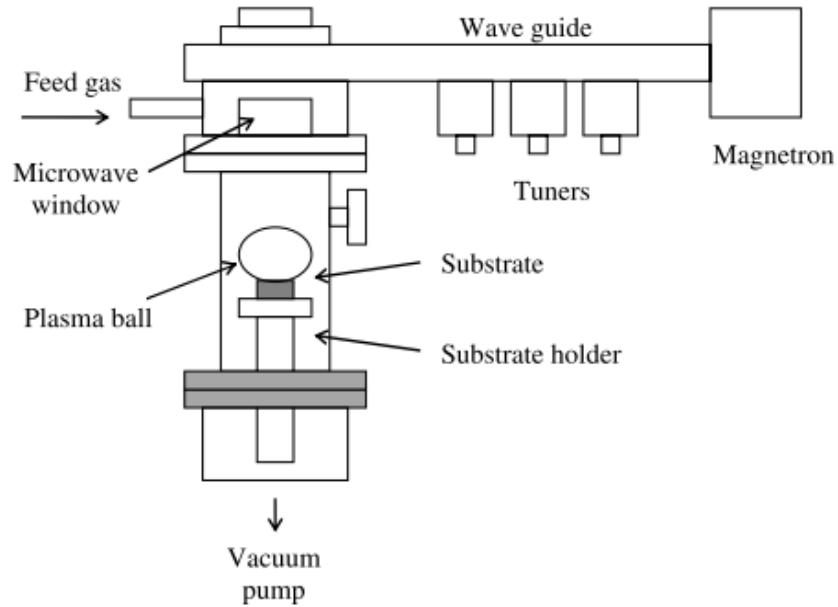
Figure 2-2. Schematic of typical MPCVD system [58].

2.2.2 Mechanism of Diamond Nucleation and Growth by CVD

The growth of diamond on single crystal diamond substrate is relatively easy and known as a homoepitaxy [48]. However, it is difficult to grow diamond on non-diamond (hetero) substrates. Diamond usually has low nucleation density on non-diamond materials [51]. With diamond seeds embedded into hetero-substrates, the nucleation of diamond can be significantly enhanced [56]. Also, heteroepitaxy growth of diamond preferentially takes place on the steps or defects [59]. The pre-scratch treatment of substrate with diamond particles has two beneficial effects on diamond nucleation: the scratching creates defects and the diamond particles are embedded as primary nuclei. The diamond nucleation can be also enhanced by a negative bias on the substrate. The incident ions have adequate energy to impinge into the substrates and react with the substrate to form a carbide layer. Also, the bias induces the emission of electron from the substrates, which enhance the plasma [60]. However, a high bias leads to the failure of deposition, perhaps due to the high ion energy damage the facet structure of diamond nuclei.

9

The chemical and physical processes during CVD are complex due to the collaboration of several aspects, such as gas and solid chemistry, heat and mass transfer, crystal nucleation and growth, thermal dynamics and diffusion. It is a challenge for the researchers to comprehensively illustrate the mechanism of diamond growth by CVD. Some common views are shown in Fig. 2-3. Firstly, a gas mixture is introduced into chamber as reactants. The most commonly used precursor is CH_4/H_2 mixture with a few percent of CH_4. The structure of diamond coatings is independent of the type of carbon-containing gases. The precursor is activated by either thermal method (e.g. hot filament) or electric discharge (e.g. microwave plasma). The gas dissociation significantly affects the growth rate of diamond. However, there is no direct evidence that the type of dissociation method would affect the structure of diamond coatings. In MPCVD, the hydrogen molecules are activated by the electric discharge into atomic hydrogen and electrons [61]:

$$H_2 + e^- \rightarrow H + H + e^- \qquad\qquad [2.1]$$

Then, the H atoms react with the hydrocarbon gas (e.g. CH_4) and generate active radicals, mainly CH_3 [62]. Sometimes the CH_2 and CH radicals can be detected due to the further reaction of H atoms and the radicals:

$$CH_4 + H \leftrightarrow CH_3 + H_2 \qquad\qquad [2.2]$$

$$CH_3 + H \leftrightarrow CH_2 + H_2 \qquad\qquad [2.3]$$

$$CH_2 + H \leftrightarrow CH + H_2 \qquad\qquad [2.4]$$

$$CH + H \leftrightarrow C + H_2 \qquad\qquad [2.5]$$

REACTANTS

$(H_2 + CH_4)$

$\Downarrow$

DISSOCIATION

$H_2 \xrightarrow{e^-, \text{heat}} 2H$

$CH_4 + H \rightarrow CH_3 + H_2$

·

·

·

FLOW AND REACTION

Diffusion
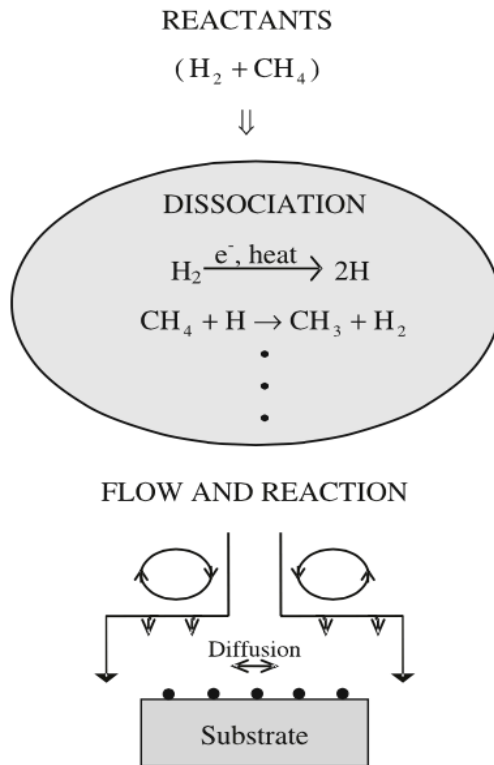
Substrate

Figure 2-3. Schematic of physical and chemical processes during diamond CVD [1].

The atoms and active radicals are transported towards the substrate. The chemical reaction of active radicals takes place in the gas phase and on the surface of substrate. When the active species incident on the substrate, they show several possible behaviors, such as absorption by the surface, desorption into the gas phase, and diffusion into the surface. The carbon films are formed when they are absorbed. If the deposition condition is suitable, diamond structure forms. As shown in Fig. 2-4, the possible explanation of the diamond growth is presented. Firstly, the atomic hydrogen extracts one hydrogen atom from the surface and molecular hydrogen forms. In the second step, another radical is absorbed at the dangling carbon bond and leads to the formation of C-C bond. Similarly, another hydrogen is removed and the radical is received by the dangling bonding. As the reaction proceeds, the diamond lattice is built up.
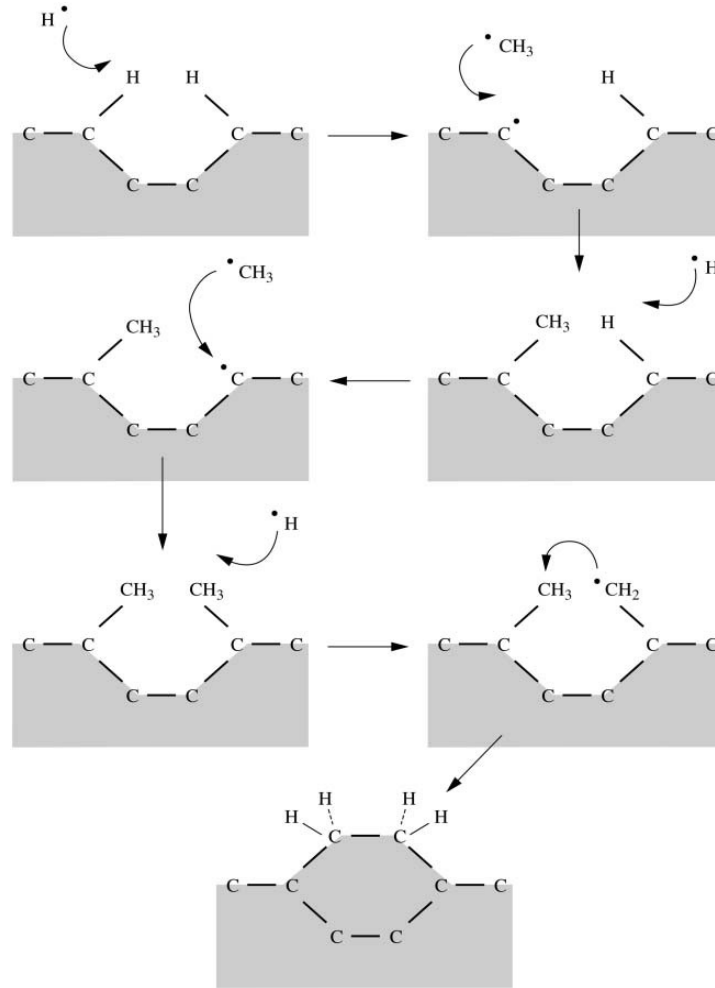
Figure 2-4. Schematic of diamond growth at a {110} trough site [63].

2.3   Characterization Techniques

2.3.1   Microscopic Techniques

1)   Optical microscopy

Microscopic techniques have been employed to observe the morphology and structure of diamond-coated samples. Optical microscopy has been developed and applied since early 17th century. This technique is inexpensive and convenient. Generally, it consists of two main glass lenses: an objective lens and an eyepiece lens. More lenses are employed to obtain higher magnification. However, the aperture of the observation lens restricted the spatial resolution,

which is up to 0.3 μm [64]. The metallurgical microscope is useful to image the microstructure of phases in metallic samples and can be used to observe the morphology of microcrystalline diamond coatings.

2)   Scanning electron microscopy

SEM is an electron beam based microscopic device, which has a better spatial resolution than optical microscopy. It is the most frequently used technique to characterize the surface morphology of diamond coatings. The image of the samples is obtained by the interaction of electrons and sample point-by-point. As shown in Fig. 2-5, the incident electron beam can be scattered in-elastically and elastically, resulting in the emission of secondary electron (SE) and the reflection of backscattered electron (BSE), respectively. Various signals are also emitted during the process, such as Auger electrons and characteristic X-rays. Either SEs or BSEs are used for imaging in SEM devices. Generally, SEs have lower energy and mean free path than BEs. The average moving distance of SEs is very short, thus, only the SEs within the depth of maximum 2 μm can be detected. The SEM based on SEs is suitable for characterization of the near surface topography. As the BEs is ejected during elastic scattering, their average energy is only slightly lower than the primary electron beam. In the kinetic point of view, the energy of BEs is affected by the atomic number of element. Therefore, BEs imaging can illustrate the contrast of variations in compositions. The characteristic X-rays also provide information of chemical composition, which is detected in Energy-dispersive X-ray spectroscopy (EDS) equipped with the SEM [65].
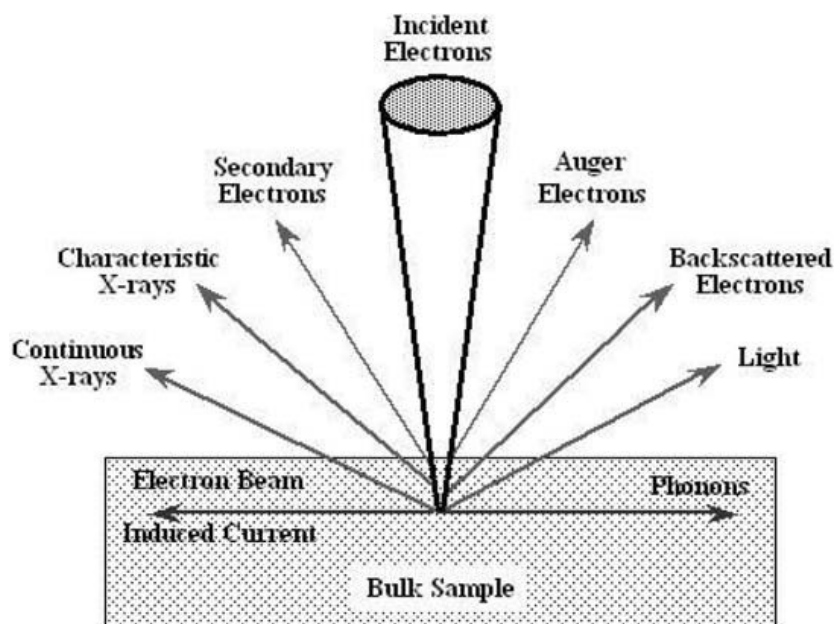
Figure 2-5. Schematic of the electron beam and specimen interaction in SEM [65].

The configuration of a typical SEM instrument is shown in Fig. 2-6. The electron beam is generated by an electron gun, such as thermionic gun (e.g. tungsten hairpin and LaB_6), Schottky electron gun, or field emission gun (FEG). The electrons are activated by heat in a thermionic gun. In the Schottky electron gun, a strong electric field is applied with heating and electrons are emitted by Schottky effect. In the FEG, applying a strong electric field on single crystal tungsten tip induces the emission of the electrons. Condenser lenses used can focus the electron beam to diameter less than 10 nm. The scan generators provide current to the coils and control them in two directions (x and y). The electrons pass through the coil in z direction due to the circular magnetic field. The electron beam is deflected in x direction and condensed by the objective lens. Thus the electron probe focuses on the specimen and performs the raster scanning. After scanning a line along x-axis, the electron beam is deflected back to start the next parallel line. The start point of line moves along y-direction. The signals of the generators are connected to the display device, such as a cathode ray tube (CRT). Also, the SEs or BEs are collected by the

14

detector and the signal is transferred to the CRT. As a result, the point where the electron probe

scans has a corresponding point on the CRT display [64].

SEM has the most popularity among various microscopy techniques. The image mode is

flexible, so that the specimen can be observed from large scale to nano-scale. Also, the display is

straightforward and understandable. Nowadays, high spatial resolution up to 0.5 nm has been

achieve in FEG-SEM. The requirement for specimen condition and preparation is relatively

accessible. Various analytical techniques can be equipped to achieve a comprehensive study.

Moreover, the operation of the instrument is user-friendly and highly automatic.
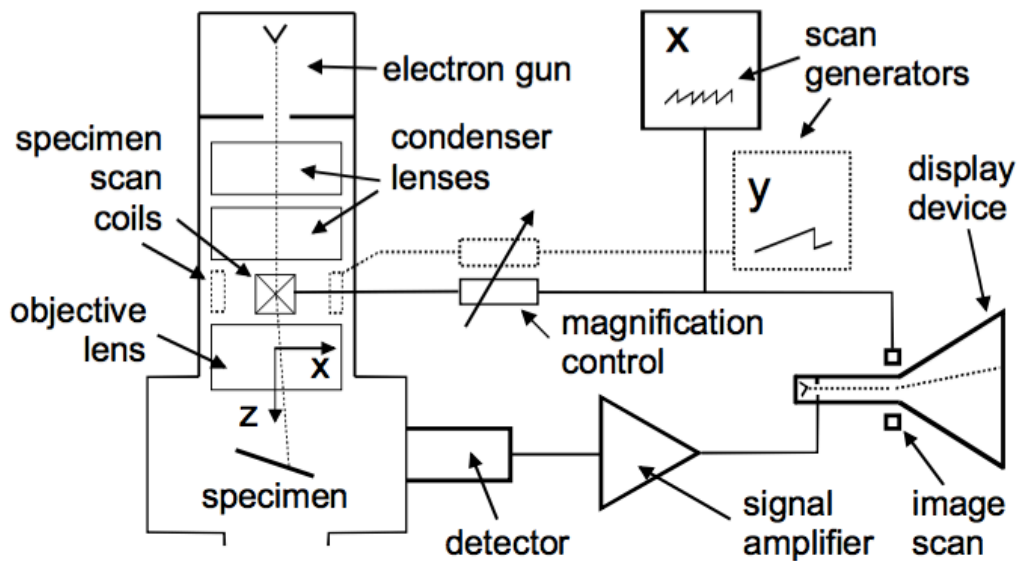
Figure 2-6. Configuration of an SEM device with a CRT display [64].

3)　　Transmission electron microscopy

TEM device usually has a higher spatial resolution than SEM. It is favorable for imaging

and analyzes interface and structures at nanometer and angstrom scales. Though the invention of

TEM was prior to SEM, it has not achieved the same popularity as SEM. The thickness of a

TEM specimen should be within hundreds of nanometers. The sample preparation is complex and time consuming, which limits the applications of TEM.

A TEM device consists of several parts, including electron gun, electron lens, apertures, specimen stage, vacuum system, and imaging system. The electron gun generates an electron beam with high energy of 80-3000 keV, which is required for electron beam to transmit through the specimen. The electrons are in-elastically and elastically scattered by the atoms. With respect to the way electron beam incident on the specimen, TEM has conventional (CTEM) mode and scanning (STEM) mode. In STEM, a scanning electron probe is used for high-resolution imaging, elemental analysis and electron diffraction. The parallel electron beam in CTEM is used for imaging and electron diffraction. The bright field (BF) is the most popular imaging method in TEM. The parallel electron beam is diffracted by the specimen or transmitted through the planes. An aperture is placed between objective lens and the imaging plane at the back-focal plane of the lens. In BF imaging mode, the transmitted beam passes through the aperture in the center, which is displayed as a bright hole. The atomic planes in the grains diffract the electron beam, which is screened as dark regions.

2.3.2 Spectroscopic Techniques

1) Energy-dispersive X-ray spectroscopy

When a high-energy electron strikes the specimen in SEM, the inner shell electron of the atom may receive enough energy during the scattering. The inner shell electron is ejected and an outer shell electron then fills the vacancy. As the electron drop from higher state to lower state, the energy is emitted as X-rays or light (Fig. 2-5). Alternatively, the energy may be transferred to another outer shell electron, which is called Auger electron. The signals of X-rays and Auger electrons are both characteristic for the elements. The generation of Auger electrons is favored in

light elements. The emission of X-rays is dominant in high atomic weight elements. The characteristic X-rays illustrate the energy difference of the two states in the element.

The characteristic X-rays are detected by two methods, which are distinguished as energy-dispersive X-ray spectroscopy (EDS) and wavelength-dispersive X-ray spectroscopy (WDS) (Fig. 2-7). In a wavelength-dispersive spectrometer (a), the x-rays are diffracted by a single crystal and then counted by a detector according to different wavelengths. The inter-planar spacing of a crystal is dependent on the element of interest, which is based on the Bragg's law. As a result, WDS detects one element at one time with a specific crystal. Instead, EDS collect all detected elements in a single spectrum. In an energy-dispersive spectrometer (b), the x-ray quanta generate charge pulses in the detector. The electric signals are processed and transformed to digital signals, which are thus designated into slots based on the energies. The EDS spectrum shows the intensity of X-rays versus photon energy. The chemical and elemental analysis can be performed as a line-scan or a map distribution. With the modern software for EDS, the overlapping peaks of different elements can be distinguished. The spatial resolution of EDS elemental distribution map is dependent on the activation volume of the incident electron beam and the mean free paths of X-ray quanta. High resolution about 100 nm can be obtained by narrowing the electron beam in SEM [66]. As a result, EDS provides elemental analysis with accuracy and high spatial resolution.
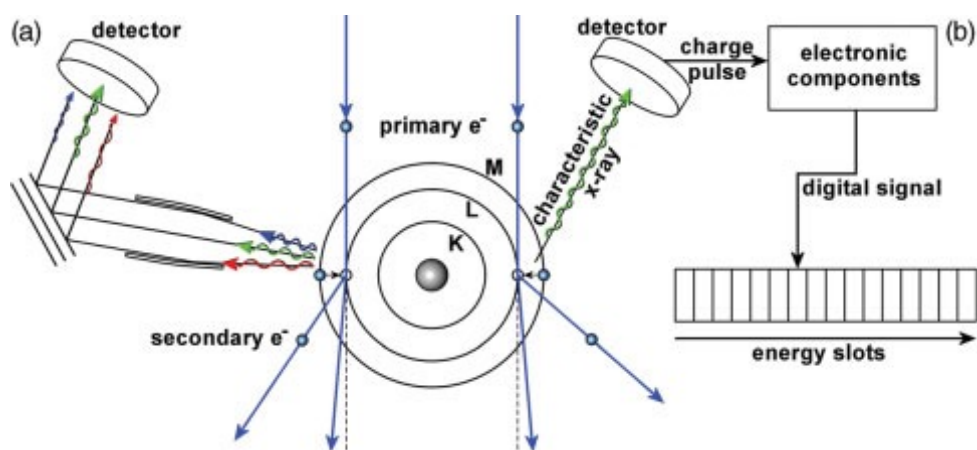
Figure 2-7. Schematics of WDS (a) and EDS (b) measurements in a SEM [66].

2)   **Raman spectroscopy**

Raman spectroscopy is commonly used to characterize the vibrational modes of the molecules. The position and the shape of the peaks are sensitive to the impurity and strain of the crystal lattice. When laser light is scattered by a molecule, most photons are elastically scattered and have the same energy as incident photons. The elastic scattering is referred as Rayleigh scattering. A small fraction of light undergoes inelastic scattering, which also called Raman scattering. The electromagnetic radiation excites the molecule to a virtual energy state before the photon is scattered. The scattered photon has lower energy than the incident photon when the molecule is excited from ground state, which is called the Stokes scattering. Thus, the frequency of the photon shifts to a lower value. In contrast, the scattered photon has higher energy than the impinging photon when the molecule is originally in an excited state, which is called the Anti-Stokes scattering. Correspondingly, the frequency of photon becomes higher than the incident radiation. The frequency shift is shown as the x-axis in a Raman spectrum. The intensity of the shift is the y-axis, which is related to the rotation and vibration state of the specimen. Generally, only the Stokes shifts are analyzed because the low frequency signals have higher intensity.
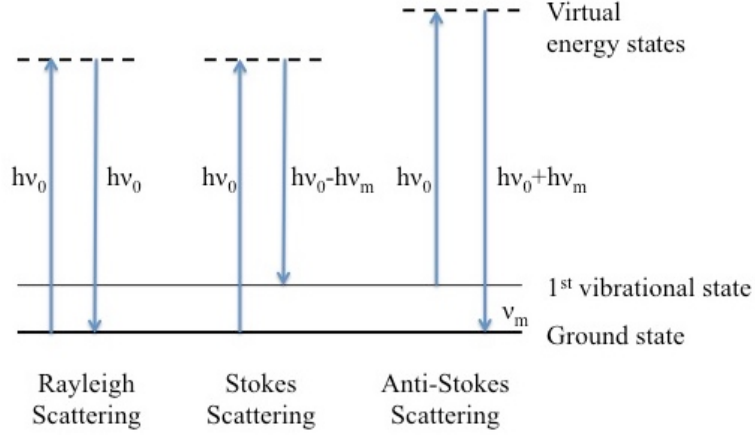
Figure 2-8. Diagram of light scattering.

Diamond has two carbon atoms in a tetrahedral primitive cell. Its high symmetric structure is Raman active and the mode are triply degenerated [67,68]. The first order peak locates at 1332 cm^{-1}, which is characterized as the diamond peak. The crystalline graphite has two Raman active modes. A low wavelength peak occurs at 1357 cm^{-1} because of a shear mode of two adjacent sheets. And a higher wavelength peak 1580 cm^{-1} is assigned to the stretching mode within the sheet. The features of diamond peak reveal its thickness, internal stress and grain size. The intensity of Raman line is proportional to the thickness. The full width at half maximum (FWHM) indicates the quality of diamond. The shifting of peak could be attributed to the residual stress within the diamond film. The downward shift of the peak could be related to tensile stress whereas the upward peak shifting could be caused by compressive stress. Quantitative relationship between the peak shift and residual stress was reported by Ager and Drory [69],

$$\sigma(GPa) = -1.08(v_s - v_0)(cm^{-1}) \quad \text{for singlet} \tag{2.6}$$

$$\sigma(GPa) = -0.384(v_d - v_0)(cm^{-1}) \quad \text{for doublet} \tag{2.7}$$

19

where υ_0 was the natural diamond peak at 1332 cm^{-1}; υ_s was the singlet shift and υ_d was the doublet shift. The equations were modified by Ralchenko et al. when the peak did not split [70]. The measured peak is in the center of the singlet and doublet peaks,

$$v_{measured} = 0.5(v_s - v_d)(cm^{-1}) \qquad\qquad [2.8]$$

So, the equation is rewritten as

$$\sigma(GPa) = -0.567(v_{measured} - v_0)(cm^{-1}) \qquad\qquad [2.9]$$

The peak shift in Raman spectrum could be induced by residual stress in diamond. The residual stress can be resulted from the mismatch of thermal expansion coefficient, which lead to the splitting and delamination of coating, and the cracking of substrate.

3)   X-ray absorption near edge structure

XANES is a type of X-ray absorption spectroscopy (XAS), which has been commonly used for characterizing surface geometric and electronic structures. The technique is based on the photo-absorption phenomenon with the excitation of the core level electrons to unoccupied states. The intense and tunable soft X-ray is generated by a synchrotron radiation. The synchrotron source produces high intensity beam through a beam line to the end-station. Also, the resultant radiation has strong polarization, which is beneficial for identifying the orientations of σ-bond and π-bond.

The photo-absorption is initialized when the energy of X-ray reaches the threshold. The energy threshold depends on the transition from the core level to the lowest unoccupied level. As shown in Fig. 2-9a, the electron in the core level absorbs the energy of an incident X-ray photon and travel to an unoccupied level. As the energy of X-ray increases, the electron can be excited to the continuum state [71]. The excitation creates a hole in the core state and a photoelectron, which is called the final state. The final state is immediately changed because an outer shell

electron fills the vacancy. The process is accompanied with the emission of an Auger electron or a fluorescent photon.

The signals are collected through the fluorescent yield (FY) or the total electron yield (TEY). The FY mode detects emitted fluorescent photons excluding the other signals. The resultant spectrum has low signal/background ratio. This method is not surface sensitive because the absorption depth of X-ray can be up to hundreds of nanometers. The cost of fluorescent detector is high and the count of the signal is sometimes low [72]. In the TEY mode, the electrodes in the detector collect all the emitted electrons, including mainly secondary electrons, as well as photoelectrons and Auger electrons. The electrons have short mean free path, which travel from a depth up to tens of nanometers. So the TEY mode is surface sensitive and not affected by the absorption of fluorescent photons. Compared to FY mode, TEY mode has advantages including surface sensitivity, simplicity, cost-effective, and low signal/noise ratio. However, the signal/background ratio of TEY is relatively high.
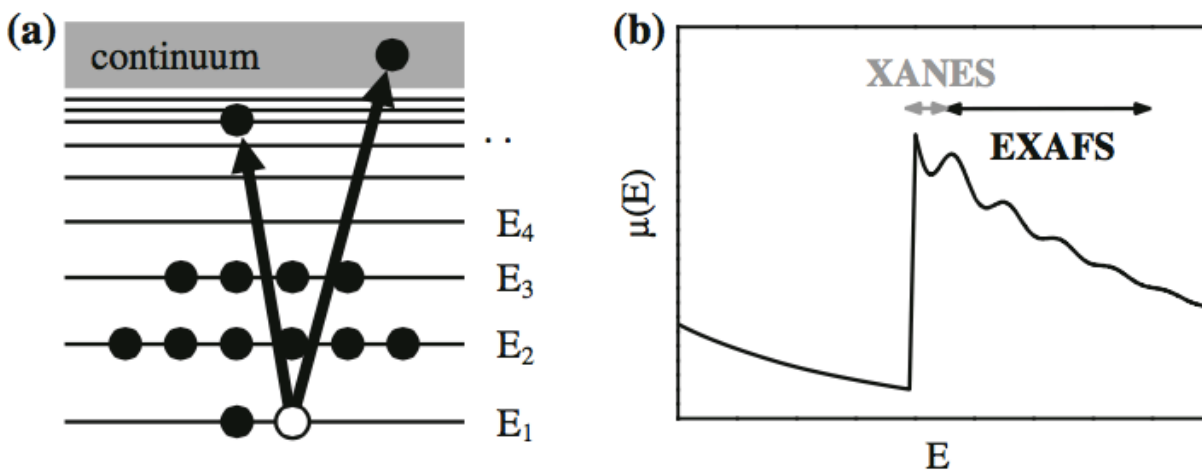
Figure 2-9. Schematic of photo-absorption process (a) and XAS spectrum with XANES and EXAFS regions (b) [71].

XANES is obtained in the region of 5-150 eV over the energy threshold (Fig. 2-9b). The corresponding electron transition is from the core level to unoccupied level. The photoelectron

undergoes the multi scattering by the neighbor atoms. Therefore, XANES provides information of the chemical bonding and crystal phases. For example, the structure of AlN has been characterized by N K-edge and Al K-edge XANES [73,74]. The extended X-ray absorption fine structure (EXAFS) is in the region of 150 eV more than the energy threshold. The electron is excite to a continuum state which is dependent of the nearest atomic arrangement. It is suitable for interatomic structural characterization.

2.3.3 Crystalline Structure Characterization

X-ray diffraction (XRD) is an analytical technique used to identify the crystalline structures. X-rays are coherent electromagnetic radiations with short wavelength (λ). Atomic planes are periodically arranged in a crystalline. The wavelength of X-ray has similar value as the planar spacing, so that the X-ray is diffracted. When X-ray impinges the atomic plane at angle θ, it is elastically scattered by the electrons, while the interaction of X-ray and neutron is negligible. The deflected waves may weaken each other via destructive interference in most orientations. The constructive interference takes place when the impinging angle meets the Bragg's law,

$$2d\sin\theta = n\lambda \qquad\qquad\qquad [2.10]$$

where d is the planar spacing, θ is the impinging angle, λ is the wavelength, and n is an integral. The scattered X-ray has high intensity where the constructive interference occurs.

A conventional XRD instrument consists of five main components: an X-ray source, the primary optic, the sample stage, the secondary optics, and the detector [75]. The X-ray tube generates X-ray from a metallic target activated by electron source. The wavelength λ of X-ray should be in the same order as the planar spacing d in order to form the diffraction pattern. The shapes of X-rays are dependent on the analytical applications. For example, the line focus beam is used for phase diagnose and point focus beam is used for texture and stress. Slits are employed

to increase the convergence of the beam. Sometimes, X-ray mirrors are introduced to create focused beam. The sample stage is a stable stand while using the rotation configuration of the tube and detector. The rotation of sample stage is used to analysis inhomogeneous structures or to neutralize the instrumental inaccuracy. The deflected beam transmits through a secondary optics, which reduces the divergence. Then, the detector receives the parallel X-ray beam, which is commonly scintillation or proportional.
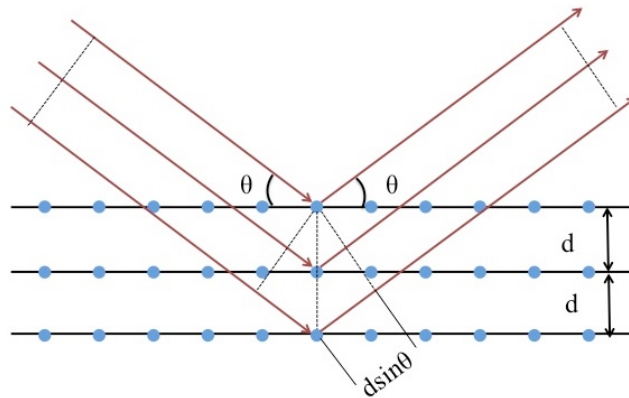
Figure 2-10. Diagram of Bragg's Law.

An XRD pattern presents the relationship of angle 2θ and the intensity of the diffracted beam. The positions of the peaks determine the lattice parameters of the phases. Also, the shape and shift of the peaks indicate the size, strain and preferential orientation. The positions of angular 2θ can be referred to the powder diffraction files. The polycrystalline diamond has a specific pattern shown in Table 2-1. In practice, the relative height of the peaks indicates the preferential grain orientation. The FWHM of the peaks is calculated in order to analysis the grain size, defects and strain. The penetration depth of X-ray into diamond is above 100 μm. As a result, the XRD pattern of diamond thin film is always used to identify the structure of diamond as well as the substrates and interlayers.

Table 2-1. XRD patterns for powdered diamond (Cu Kα radiation, λ= 1.5405Å) [1].

hkl	d	2Theta	Relative intensity
111	2.0600	43.9	100
220	1.2610	75.3	25
311	1.0754	91.5	16
400	0.8916	119.5	8

2.3.4   Adhesion Evaluation

From thermodynamic point of view, the work (W_A) required to detach two phases from the interface is written as,

$$W_A = \gamma_f + \gamma_s - \gamma_{fs} \qquad [2.11]$$

where γ_f and γ_s are the specific surface energy of the film and substrate, respectively. γ_{fs} is the interfacial energy [76]. For example, the interfacial energy of a film and its homogeneous substrate is zero, thus $W_A = 2\gamma_s$. The positive value of W_A indicates the adhesion or attraction. The adhesion of an epitaxial coating and its substrate are the strongest. The value of γ_{fs} is important for the adhesion failure at the interface of different materials. The interface of solid-solution formers has higher adhesion than the interface of immiscible materials forming chemical bonding. From atomic point of view, the adhesion energy is either due to the van der Waals force or due to chemisorption, such as covalent, metallic and ionic binding.

Film and substrate interfaces have been classified into four types: 1) Abrupt interface is identified by the absence of interaction between the substrate and film, e.g. diamond on copper substrate; 2) Compound interface is usually the few atomic layers with both the film and substrate materials, e.g. Al on steels; 3) Diffusion interface is identified by a gradient layer due to the solubility between the film and substrate materials; and 4) mechanical interface is recognized as the mechanical interlocking between a film and a rough substrate.

Nevertheless, the actual interfacial binding strength is very hard to be directly measured. Various techniques have been used to evaluate the adhesion, including pull-off tests, scratch tests and indentation tests. Pull-off testing is a quantitative test using a pulling force on an adhesive above the coating. The method is accurate if successfully calibrated. The main disadvantage is the strength limitation of the adhesive, which may fail before the detachment of diamond coating. The scratch testing is a qualitative method using an indenter under a perpendicular force. The shape of the indenter is known and the load is continuously increasing. The scratch is observed by using a microscopic technique to determine the critical load. The acoustic signals are also measured to estimate the critical load for detachment. The acoustic emission increases significantly the coating is detached from the substrate. However, the scratch tips undergo wear and cleavage while used on hard coatings. Another qualitative method, indentation testing, is simple and eliminates the potential damage to the indenter. There are two approaches to estimate the adhesion. One is to determine the critical load that induces the delamination. The other is to compare the imprint of the delamination area. For example, Rockwell C indentation testing is using a spherical coned diamond tip. The imprint after applying a load 150 kg can be observed under an optical microscopy. The delamination is classified into HF 1 to HF 6, where only HF 1 and HF 2 indicate satisfying adhesion. Also, a range of loads can be applied on the coating to estimate the critical load for delamination.

2.4   Deposition of Diamond Coatings on Fe Based Materials

2.4.1   Diamond Deposition on Bare Fe Based Substrates

In 1976, Kanda et al. synthesized crystalline diamond on pure iron by HPHT [77]. With the development of CVD techniques, researchers have tried to deposit diamond coatings on various Fe-based materials. It has been found that there are three main barriers. Firstly, carbon

dissolves into the Fe substrates readily during the deposition and thus the substrate surface has a low carbon concentration until the carbon is saturated inside the substrates. This prolongs the time for diamond nucleation and changes the structure of the substrates and thus negatively impacts the properties of the substrates. Secondly, the formation of graphite soot is inevitable on Fe based materials because Fe catalyzes the formation of graphitic carbon. The soft graphite phase formed at the interface results in a weak adhesion between diamond and substrates and introduces impurity into diamond coatings. Lastly, there is a large mismatch of coefficients of thermal expansion (CTE) between diamond and most of the Fe based materials. At room temperature, the CTE of diamond is 1×10^{-6} K^{-1}, while CTE of steel is about 16×10^{-6} K^{-1}. The large mismatch induces a large thermal stress within the interfaces, which can thus cause the delamination [6]. The thermal stress of diamond can be derived as,

$$\sigma_{thermal} = \frac{E}{1-\nu} \int_{20}^{T} (\alpha_f - \alpha_s) dT \qquad [2.12]$$

where E is Young's modulus of diamond (~1050 GPa); υ is the Poisson ratio of the diamond (~ 0.07); α_f and α_s are the thermal-expansion coefficients of the diamond film and substrate, respectively; and dT is the deposition temperature minus room temperature [69].

2.4.2 Alloying and Surface Modification on Diamond Growth and Adhesion

Liao et al. [78] deposited diamond on low carbon steel with diamond powder pre-treatment. They reported a low nucleation density of diamond and suggested the use of surface modification to enhance nucleation and adhesion. Davanloo et al. used C^{3+} and C^{4+} ions to treat the surface of stainless steel (SS) 316L and diamond coatings were then successfully synthesized onto the treated steel due to the formation of a carbide interfacial layer [79]. In 2001, Borges et al. modified the surface of SS304 by nitriding and carbonitriding [80]. They stated that Fe_xN_y and $Fe_xN_yC_z$ phases deactivated the catalytic effect of Fe and less graphite soot formed and

26

instead a composite layer of diamond, chromium carbide and chromium nitride formed at the interface and the interfacial adhesion was enhanced. Ion beam nitriding was applied to treat SS 440C by Shang et al. in the same year and it enhanced the diamond nucleation but did not eliminate the formation of graphite at the interface [10]. In 2004, Buijnsters et al. obtained continuous diamond coating on borided SS316 substrates and the critical load in scratch testing was 69 N, which is not sufficient for most of the applications [81]. Gowri et al. modified the deposition process to three steps in a HFCVD reactor and improved the nucleation of diamond on tool steel [82]. The same group also reported that boriding high-speed steel could reduce the formation of graphite at the interface [83]. Recently, boriding treatment was used on SS316 and nanostructured diamond (NSD) was deposited on the treated SS316 and SS 440C [11].

Substrate composition had significant influence on diamond growth [9,84]. For example, well adherent diamond coating has been deposited on chromized 41Cr4 steel [85]. The addition of Si and Al to Fe-9Cr alloys enhanced diamond growth [86]. However, the addition of Mo, Cr, Mn and Ti to Fe-15Cr alloys had no obvious effect on promoting diamond growth. It has been found that only Al can significantly enhance diamond growth on Fe-Cr alloys [12,86]. The addition of a small amount of Al into Fe based alloys can enhance the quality of diamond coatings [87]. The enhancement mechanism of Al and Cr in Fe based materials has been further studied and the results show that the Al oxide layer formed on the surface can prevent the diffusion of carbon and suppress the catalytic effect of Fe [88]. For Al alloyed ferrous substrates, a nano-scale aluminum oxide buffer layer forms at the interface and inhibits the carbon diffusion [23,89]. Due to the third element effect of Cr, the critical content of Al to enhance diamond growth can be reduced. Cr has been found to be beneficial for interfacial adhesion with the formation of carbides [23]. The barrier effect of Cr is attributed to the formation of an intense

chromium carbide layer. The carbide layer promotes the carbon saturation at the surface and the following nucleation of diamond. Also, the chromium carbide phase suppressed the catalytic effect of Fe by physically separating it from the reaction atmosphere [15].

Chromium is also an important alloying element in ferrous alloys and it has been considered a potential interlayer material to improve diamond deposition on steel substrates. The effect of Cr in ferrous alloys with a low fraction (< 20 wt.%) of Cr has been studied, and the results show that Cr has little effect on diamond nucleation and growth [12,23]. Using Cr as interlayer was reported to be successful in improving the adhesion of diamond film on steels [15,24,25], primarily attributed to the formation of chromium carbides. On the other hand, other researchers concluded that Cr did not successfully function as a good interlayer for diamond deposition on ferrous alloys [26]. In one word, Cr is important for diamond deposition but the effect of Cr in ferrous alloys on diamond nucleation and growth has not been clarified. To clarify the effect of Cr on the nucleation and growth of diamond on ferrous substrates, in present work, a series of Fe-Cr binary alloys with a wide range of Cr content has been prepared, and the corresponding nucleation and growth behavior of diamond was investigated in a microwave plasma enhanced CH_4-H_2 atmosphere, which has not been reported in previous research.

2.4.3 Diamond Deposition on Fe Based Substrates with Interlayers

Intermediate layers are inevitable in order to deposit well adherent and high quality diamond coatings on Fe based substrates. Efficient interlayers act as barriers to suppress carbon diffusion into substrate and the catalytic effect of Fe for graphitic carbon formation. The interlayers also provide active nucleation sites and strong bonding for diamond coatings. Extensive research has been done to develop appropriate interlayers experimentally [21,22,90–94]. A few papers have also tried to estimate the effect of a single metallic interlayer on the adhesion of diamond coating theoretically [95–97]. However, the performance of an interlayer

28

system is complex and dependent on many aspects: the affinity with carbon and strength of carbide bonding; the structure, composition and thickness of interlayers, the combination of multi-interlayers, and the thermal expansion coefficient. Theoretical calculations are hard to predict the behavior of an interlayer system.

Various single interlayers have been studied. W interlayer was applied on #R18 steel for diamond deposition [70]. The diamond coatings did not delaminate instantly but had high internal stress because the mismatch of CTE is still high with W interlayer. Ti interlayer was applied on steels by Fan et al. [98] and both Ti and Cr were applied on steel and cast iron for diamond deposition by Silva et al. and Fan et al. [24,99]. The results show that both interlayers could provide good nucleation sites for diamond and the adhesion varies with the deposition parameters and substrate materials. Ti interlayer shows better adhesion than Cr interlayer, which can be attributed to the stronger bonding of TiC. Diamond composite interlayers on high-speed steels show better adhesion than a single silicon carbide interlayer due to the composite structure and the formation of carbide phase [94]. Diamond nucleation density was too low on Si coated steel to form continuous coatings [100]. Various Ti and Zr based compound interlayers have also been investigated on high speed steel [16]. The results show that TiC is the best interlayer where ZrN, ZrC, and TiC/Ti(C,N)/TiN interlayers are not suitable. Haubner et al. investigated various physical vapor deposition (PVD) interlayers including TiN, CrN, TiAlN and TiCN on 18/9-CrNi steel and have found that TiN, TiAlN and TiCN are better carbon diffusion barrier than CrN [101]. High velocity oxy-fuel sprayed thick WC-Co interlayer (>10 μm) on high-speed steel and AISI 1085 carbon steel has been found to be effective in reducing formation of graphite and enhancing diamond nucleation and adhesion. [83]. Wei et al. studied the effect of the thickness and structure of WC-Co interlayers on the wear and corrosion resistance of diamond coatings.

The results demonstrate that diamond coatings hold potential application for corrosion and wear protection applications [102,103].

Cr based interlayers have attracted special interest. Fayer et al. used chromium nitride interlayer on carbon chrome steel and achieved desirable adhesion and wear resistance (critical load of Rockwell C indentation was 1000 N) due to the formation of chromium carbides [104]. However, Buijnsters et al. reported that diamond could not form continuous coating on Cr-N coated SS316 due to the large CTE of the substrate [19] but could form on PVD CrN interlayer because of the reduced thermal stress [81]. CrN interlayers have been further studied by other researchers [41,105]. Diamond coatings on metallic Cr coated 41Cr4 and X50CrMoV15 substrate showed high nucleation density and high growth rate on due to the formation of a chromium carbide interlayer during diamond deposition [25,106]. Further tribological evaluation of diamond deposition on chromium carbide coated C35 steel suggests that chromium carbide is an effective interlayer for diamond deposition [107].

Enhancement of diamond deposition has also been achieved by using Al based single interlayers. In 1996, high purity diamond coatings was reported to be successfully deposited on ultrathin AlN coated bearing steel and tool steel [20] and on Al-N coated #45 steel [22]. In our group, diamond deposition on Al coated Fe based substrates has been systematically investigated and adherent diamond coatings have been achieved [17,21,88,108,109]. Al has high affinity with carbon [88] and can suppress the catalytic effect of Fe [17], therefore, the Al interlayer improves the quality and adhesion of diamond coatings. In our recent research [89], an annealing post treatment was employed to aluminize the substrate before diamond deposition and high resolution TEM observation of the interface suggests that Al is oxidized to form aluminum oxide

layer, which actually contributes to the enhancement of diamond nucleation and adhesion. It should be noted that Al is soft and easy to be damaged; its continuity is hard to be guaranteed.

Multilayers Mo/Ni/Mo and single layers of Mo or TiN on tool steel SKD61 have been investigated as well and the results illustrates that Mo/Ni/Mo is better than other layers [110]. An ultrathin dual layer of Al/W has found to be very effective in enhancing diamond nucleation and adhesion. In Al/W dual interlayers, the inner Al layer successfully suppressed the carbon diffusion and catalytic effect of Fe for graphite formation. The upper W layer is more effective in enhancing diamond nucleation than other carbide forming elements [21]. Meanwhile, strong bonding between WC and diamond contributes to adhesion enhancement of diamond. However, Al/Ti and Al/Cr dual layers failed to improve the adhesion of diamond [108]. In general, multilayers can combine the beneficial effects of individual layers; nevertheless, multilayers are more complicated with more interfaces and thus need careful design.

AlN is harder than W, Ti and Cr. The relatively high hardness of AlN would prevent the failure of Al layer during the pre-treatment process. In addition, AlN has a lower thermal expansion coefficient than W, Ti, Cr, and Al, which is expected to reduce the residual stress of diamond coatings. Furthermore, it has been reported that AlN interlayer can enhance diamond nucleation on steels, Si, and WC-Co [20,22]. Considering those three points, Al/AlN dual layers would be very promising to prevent the carbon from diffusion into substrates and the formation of graphite at the interface as well as reduce the residual interfacial stress induced by the mismatch of thermal expansion coefficients. Therefore, this research aims to use Al/AlN double interlayers to enhance the nucleation and adhesion of diamond on Fe based materials (SS316 and Kovar), which has not been reported in previous research. As reference, Al monolayer is also studied.

CHAPTER 3
EXPERIMENTAL METHODS

3.1   Deposition of Diamond Coatings on Fe-Cr Alloys

3.1.1   Substrate Materials and Pre-treatment

The Fe-Cr alloys were prepared by vacuum arc-melting using appropriate mixtures of pure Fe (99.79 wt.%) and pure Cr (99.86 wt.%). The nominal chemical compositions (in wt.%) of the Fe-Cr alloys were Fe-20Cr, Fe-40Cr, Fe-50Cr and Fe-80Cr, respectively. The actual compositions (in wt.%) of the Fe-Cr alloys were determined by energy dispersive X-ray spectroscopy to be Fe-20.2Cr, Fe-39.7Cr, Fe-50.4Cr and Fe-79.8Cr, respectively. The melted alloys were casted and then annealed at 700 °C for 20 h to stabilize their microstructures. After that, the alloys were cut into specimens with dimensions $10 \times 10 \times 1$ mm^3. All the specimens for diamond deposition were prepared by Dr. Yuanshi Li. Prior to deposition, the samples were abraded up to 800 grounding grit and ultrasonically cleaned in ethanol followed by distilled water. To facilitate diamond nucleation, some alloy samples were also pre-scratched ultrasonically by diamond suspension (particle size of 2 μm) for 45 min. The samples were then ultrasonically cleaned in acetone for 15 min.

3.1.2   Deposition of Diamond Coatings

Diamond deposition was performed in a 2.45 Hz MPCVD reactor (Plasmionique Inc.) as shown in Figure 3-1. The microwave power was 900 W and the substrate temperature was approximately 680 °C. The system was pumped to a base pressure of 1×10^{-6} torr and then a gas mixture of CH_4/H_2 was in introduced to the chamber at a total flow rate of 200 torr with 1 vol.% CH_4. During deposition, the working pressure was maintained at 23 torr.

3.1.3 Characterization Techniques

The deposited samples and the microstructural changes of the substrate were characterized using Raman InVia device (Renishaw 2000, Ar laser 514 nm wavelength) as shown in Figure 3-2 and X-ray Diffractometer (XRD, Rotaflex Ru-200) as shown in Figure 3-3 with Co K_α radiation. The morphologies of the deposited samples were observed by Scanning Electron Microscope (SEM, 20 kV, JSM 840 A) as shown in Figure 3-4 and Transmission Electron Microscopy (TEM, Phillips CM10) as shown in Figure 3-5. The cross-sectional images and chemical compositions were obtained by a Hitachi SU6600 SEM equipped with an Energy Dispersive X-Ray Spectroscope (SEM/EDS). Prior to the observation by SEM/EDS, the samples were ground by #800 SiC sandpaper followed by 9 μm and 3 μm diamond slurry and then etched in a 20% HCl solution for 15 seconds.

Figure 3-1. A picture of the MPCVD system (Plasmionique Inc.).

Figure 3-2. A picture of Raman spectroscopy instrument.

Figure 3-3. A picture of XRD instrument.
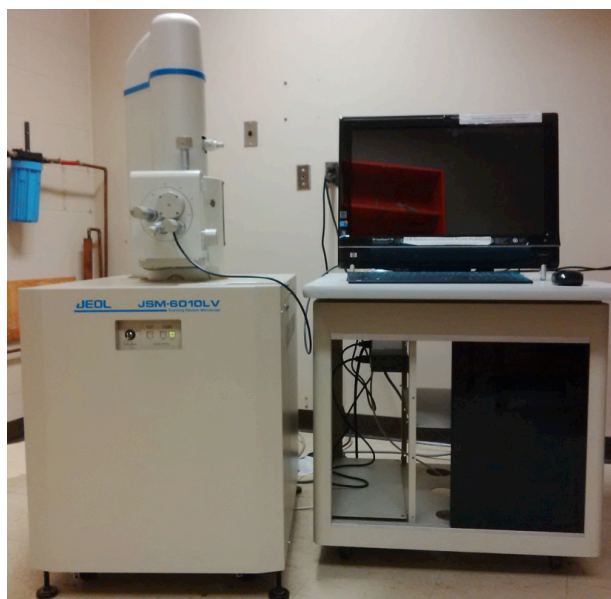
Figure 3-4. A picture of SEM instrument.

Figure 3-5. A picture of TEM instrument.

3.2　Deposition of Diamond Coating on SS316 and Kovar

3.2.1　Substrate Materials and Pre-treatment

Commercial Kovar alloy (Fe29Ni17Co, in mass %) was cut into specimens of 10 mm×
10 mm × 1 mm. AISI type 316 austenite stainless steel (SS316) sheets was also used as
substrates, which have a size of 18 mm in diameter and 1 mm in thickness. All the substrate
samples were grounded and mechanically polished with #800 SiC sandpaper and then
ultrasonically cleaned by acetone.

3.2.2　Deposition of Interlayers and Diamond Coatings

Al and Al/AlN interlayers were deposited by ion beam sputtering using an End-Hall (EH)
ion source KRI EH-1000 (manufactured by Kaufman & Robinson, Inc. USA), as shown in
Figure 3-6. In the case of preparation of Al interlayers, the Fe based samples were firstly etched
using Ar ion beam for 15 min and then coated with Al layer by sputtering Al target (purity
99.99%) using Ar ion beam with an energy of 400 eV, or AlN layer by sputtering Al in N_2
atmosphere. For Al monolayer, the deposition time was 6 hrs (if not specified). For Al/AlN dual
layers, the deposition time for Al layer or Al/AlN layers was 3 hrs respectively (if not specified).

The samples coated by interlayers were then ultrasonically scratched in a diamond
(average particle size of approximately 2 μm) suspension for 120 s. After that the scratched
samples were ultrasonically cleaned in acetone for 300 s and put into the vacuum chamber to be
deposited with diamond for 6 hrs. Diamond deposition was performed in a 2.45 Hz microwave
plasma enhanced chemical vapour deposition (MPCVD) reactor (Plasmionique), as described in
previous papers [36,111]. The power of microwave was 800 W and the substrate temperature
was approximately 670 °C. CH_4-H_2 gas mixture with 1 vol% CH_4 was introduced into the
chamber at a total flow rate of 200 sccm. A pressure 3.07 kPa (23 torr) was maintained during
the whole 6 hrs deposition.
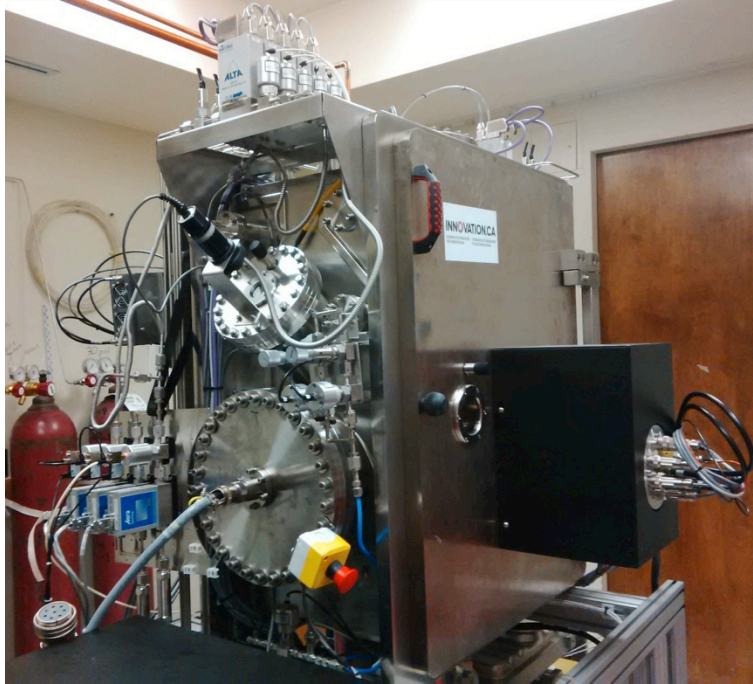
Figure 3-6. Pictures of the EH-IBD system, chamber (a) and control and power system (b).

3.2.3   Characterization Techniques

Four different kinds of samples were prepared prior to the diamond deposition: Al coated

SS316, Al/AlN coated SS316, Al coated Kovar and Al/AlN coated Kovar. The as-deposited

diamond samples were characterized by Scanning Electron Microscopy (SEM, 20kV, JSM

840A), Raman (Ar laser with wavelength of 514nm), X-ray Diffractometer (XRD, Co Kα

radiation), and Rockwell C indentation testing (load at 1470 N). The X-ray absorption spectra (XAS) at N and Al K-edge of the synthesized AlN interlayer were measured using SGM beamline at the Canadian Light Source, and the data were collected with a total electron yield (TEY) method.

4.1 Metal Dusting, Carburization and Diamond Deposition on Fe-Cr Alloys in CH_4-H_2 Plasma Atmospheres

4.1.1 Metal Dusting and Carburization of Low Cr Alloys

After exposure to the CH_4-H_2 plasma, the Fe-Cr alloys showed quite different deposition behaviors depending on their individual Cr concentrations. On the Fe-20Cr sample, a thick carbon deposit was quickly formed on the substrate surface after 3 h deposition, containing both fine graphite particles and filaments with a loosely packed structure (Fig. 4-1a). Diamond phase is not detected on this surface as revealed by Raman spectroscopy. The TEM images (Fig. 4-1b-d) further indicate that the filaments are kinds of multi-walled carbon nano-tubes embedded with metal-rich particles. Fig. 4-2 shows the cross sectional SEM/EDS results of the Fe-20Cr substrate after 3 h deposition. A carburized layer with a thickness of approximately 20 μm can be clearly seen. The elemental distribution from the surface into the substrate was carried out in the colored area labeled as 'Map 1'. Elemental spectra by EDS were also obtained for areas 'Map 2' and 'Map 3', respectively. The chemical compositions of the regions were shown in Table 4-1. It can be see that high carbon concentration has been detected from the surface till to an innermost porous layer which has a composition of 59.26% Fe, 28.35% Cr, 9.23% C, and 3.15% O (wt.%). An intermediate layer adjacent to this porous layer is rich in Cr with a composition of 58.11% Cr, 21.92% Fe, 13.39% C, and 6.58% O (wt.%). The outermost layer is basically a carbide mixture of both Fe and Cr.

With prolonged deposition times, the carburization zone becomes deeper and shows an irregular interface where substrate has been significantly degraded (Fig. 4-3). Meanwhile, diamond nucleation, with a very low density, is initiated on the substrate surface after a longer

deposition time, as shown in Fig. 4-4. It should be mentioned that a continuous diamond film could be eventually formed on this substrate after a long–time deposition. However, as the diamond nucleates and grows on an intermediate graphite soot layer, it normally possesses a weak interfacial adhesion with the underlying substrate [23]. In comparison with Fe-20Cr, the graphitization on Fe-40Cr is far less and the orientation of diamond nuclei becomes more apparent (Fig. 4-5). Similar characteristics are obtained for the Fe-50Cr substrate and the results are not shown here.
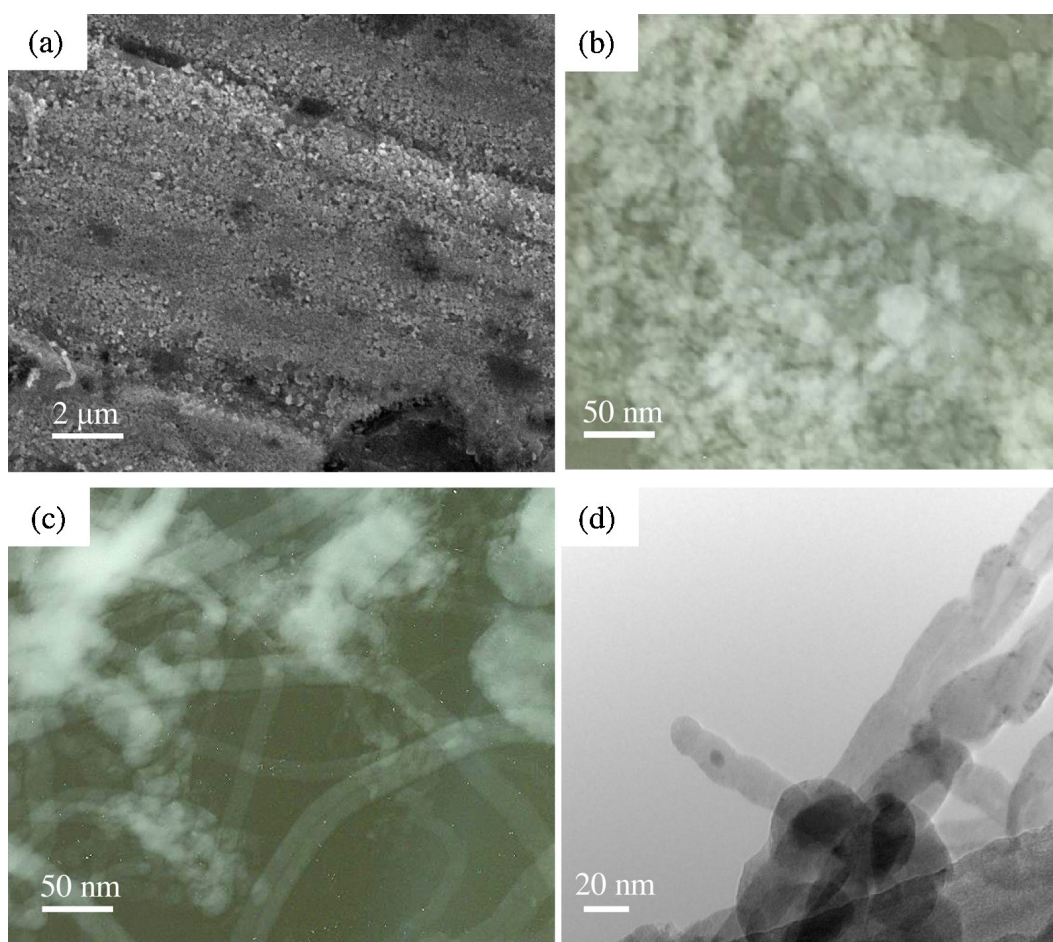
Figure 4-1. SEM image (a) and TEM images (b, c, and d) of the surface deposits formed on Fe-20Cr after exposure to CH_4-H_2 plasma for 3 hrs.
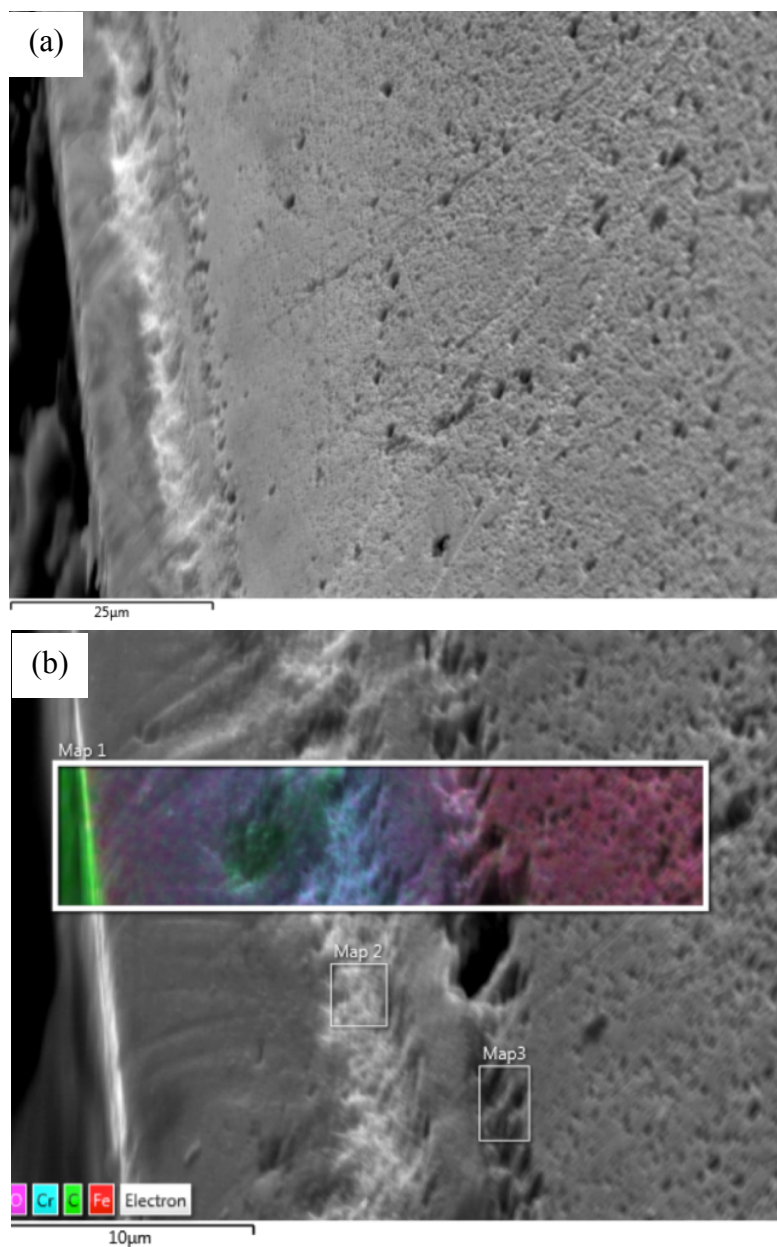
Figure 4-2. Cross-sectional SEM image (a) with corresponding EDS elemental mapping (b) of Fe-20Cr after exposure to CH_4-H_2 plasma for 3 hrs.

Table 4-1. Chemical compositions by EDS of the regions labeled in Fig. 4-2b, wt.% (wt.% sigma).

Element	C	O	Cr	Fe	Total
Map 2	13.39 (0.13)	6.58 (0.14)	58.11 (0.17)	21.92 (0.14)	100
Map 3	9.23 (0.08)	3.15 (0.08)	28.35 (0.09)	59.26 (0.11)	100
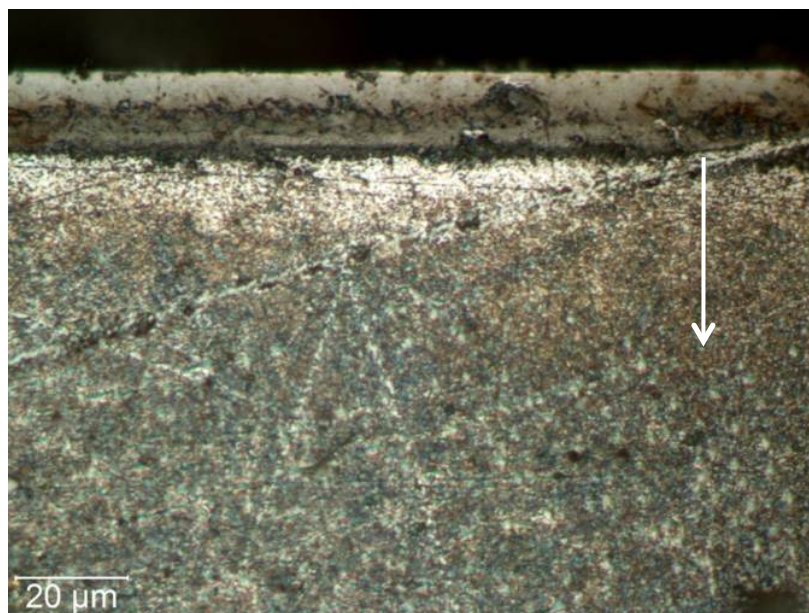
Figure 4-3. Cross-sectional metallurgical image of Fe-20Cr after exposure to CH_4-H_2 plasma for 8 hrs.
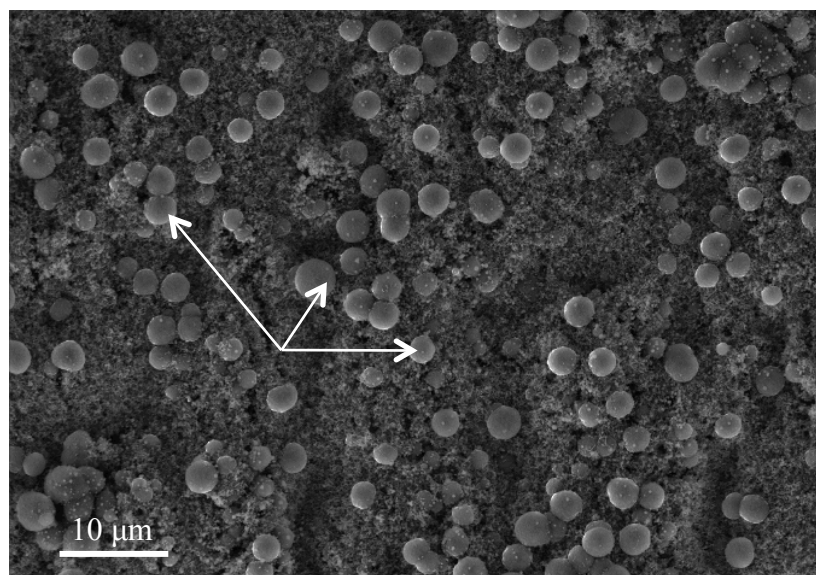
Figure 4-4. SEM image of surface deposits formed on Fe-20Cr after exposure to CH_4-H_2 plasma for 12 hrs.
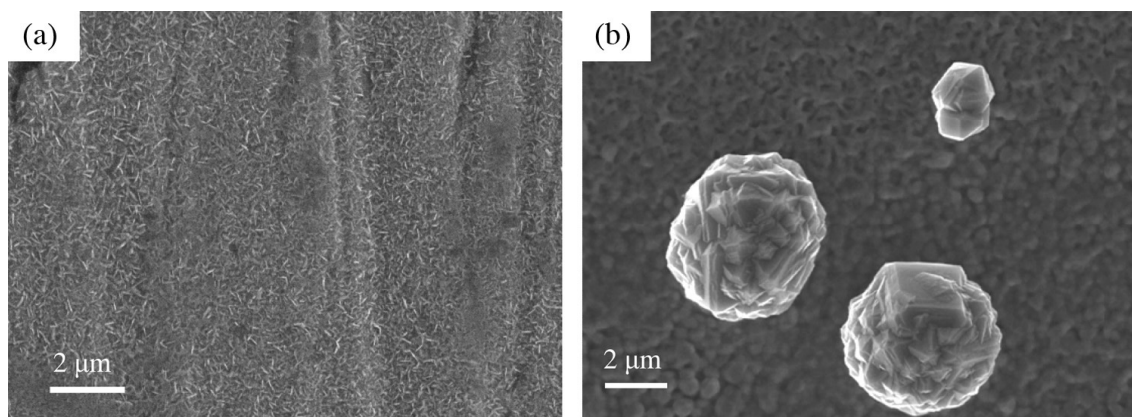
Figure 4-5. SEM images of surface deposits formed on Fe-40Cr after exposure to CH_4-H_2 plasma for 3 hrs (a) and 10 hrs (b), respectively.

4.1.2 Diamond Growth on High Cr alloy

With a high Cr content of 80 wt.%, the deposition behavior is completely different from the other Cr alloys. Figure 4-6 shows the SEM images and Raman spectra of the surface of diamond deposited on Fe-80Cr after 3-hour processing. From a low magnification image (Fig. 4-6a), crystalline diamond is observed as bright particles. Some particles are connected to lines or local clusters whereas bare substrate is shown as the dark background. From a higher magnification image (Fig. 4-6b), the average size of diamond particles is measured to be 1~2 μm, with a diamond particle density (DPD) of approximately 8×10^6 particles/cm^2. The corresponding Raman spectra were taken from two different sites on the surface. The spectra collected from the surface particles (see Fig. 4-6c) shows a clear peak centered at 1332 cm^{-1}, a typical characteristic of sp^3-bonded diamond structure, while the peaks related to graphitic carbon were not detected. And the spectra collected from the exposed alloy surface area, which is not covered by any diamond particles, does not show any graphite-related peaks (see Fig. 4-6d). This implies that the formation of graphitic species on this high-Cr alloy substrate has been effectively inhibited. These data confirm that an exclusive diamond phase has developed quickly on the Fe-80Cr

substrate. To enhance diamond nucleation and growth, a scratching pretreatment by diamond paste was performed.
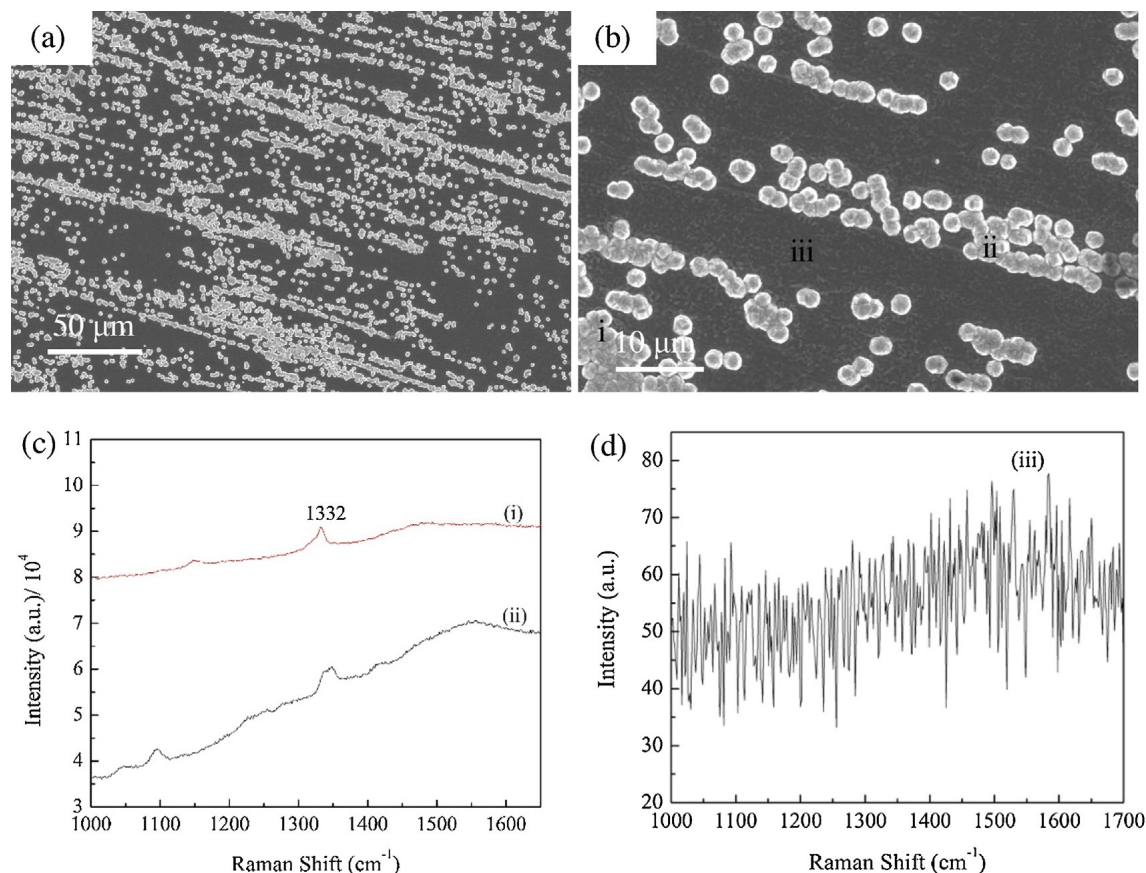
Figure 4-6. SEM images (a, b) of surface deposits formed on Fe-80Cr after exposure to CH_4-H_2 plasma for 3 hrs, and Raman spectra (c, d) of diamond (i, ii) and exposed Fe-80Cr surface (iii) as labeled in (b).

Figures 4-7a-b show SEM images of diamond films formed on Fe-80Cr after 3 h deposition on the alloys after such a pre-treatment. As expected, diamond nucleation density has been dramatically improved and a nearly continuous faceted diamond film forms. The corresponding Raman spectra indicate that the diamond characteristic peak has slightly shifted to a higher wavenumber from its standard position of 1332 cm^{-1}. This is attributed to the accumulated compressive stress in the diamond film when it is well adherent to the substrate

which has a higher thermal coefficient of expansion, indicating an enhanced interfacial adhesion [12].
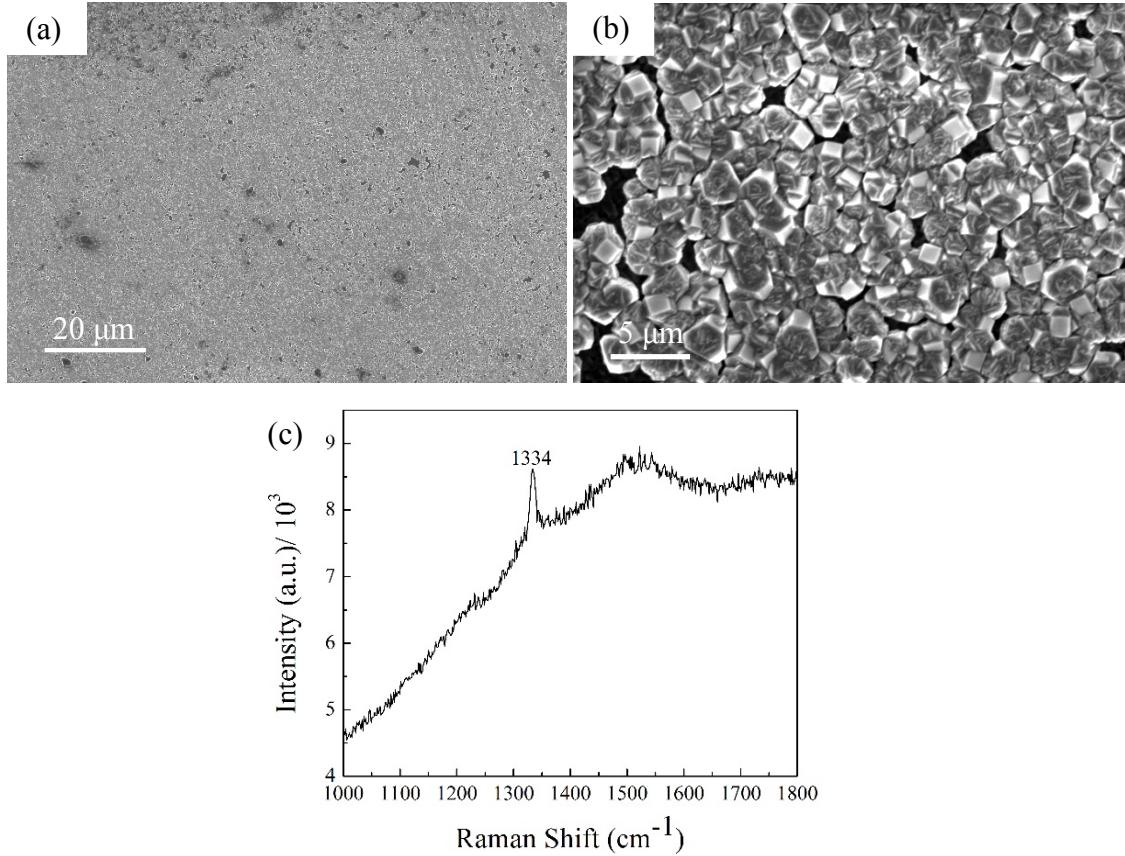
Figure 4-7. SEM images (a, b) and Raman spectrum (c) of continuous diamond film formed on Fe-80Cr with a pre-scratch treatment after exposure to CH_4-H_2 plasma for 3 hrs.

4.1.3 Effect of Cr on Substrate Carburization and Diamond Growth

Figure 4-8 shows a comprehensive comparison of the surface deposits and the changes in the substrate structures after a short time exposure to the CH_4-H_2 plasma environment. From XRD analysis (Fig. 4-8a), a carbide mixture consisting of both Cr and Fe was detected at the surface of the Fe-Cr alloys up to 50 wt.% Cr, and the relative intensity of iron carbide decreases with increasing Cr concentration in the substrates. The corresponding Raman spectra are shown in Fig. 4-8b. Two broad peaks located at 1345 cm^{-1} and 1585 cm^{-1} in the spectra (i)-(iii) of Fe-20Cr, Fe-40Cr and Fe-50Cr inclusive, verifying the existence of amorphous carbon and graphite

observed by SEM. This indicates that even with a Cr concentration of 50 wt.%, the catalytic effect of Fe for the formation of graphite has not been effectively eliminated. In contrast, only a sharp peak located at 1332 cm^{-1}, characteristic peak of diamond phase, was observed in spectrum iv taken from the diamond deposited on Fe-80Cr. Considering that graphite has 50 times more Raman scattering cross-section area than diamond [67], the concentration of graphite phase formed on the Fe-80Cr substrate should be very low, indicating that the diamond obtained has is of purity. After a long deposition time of 8 hrs, the amount of carbide phases formed become more significant for all the alloys investigated. As shown by an XRD analysis in Fig. 4-9, carbides of iron and chromium including Fe_3C, $Cr_{23}C_6$ and Cr_3C_2, have been formed on the Fe-20Cr and Fe-40Cr substrates. When the Cr content is increased from 20 wt.% to 40 wt.%, the peak intensities of Fe_3C and Cr_3C_2 decrease, while the relative intensity of $Cr_{23}C_6$ increases. This is especially evident for the Fe-80Cr substrate which shows the highest amount of $Cr_{23}C_6$ in addition to the detectable amounts of crystalline diamond. However, iron carbide and other Cr_xC_y phases, like Cr_3C_2, were no longer detected.
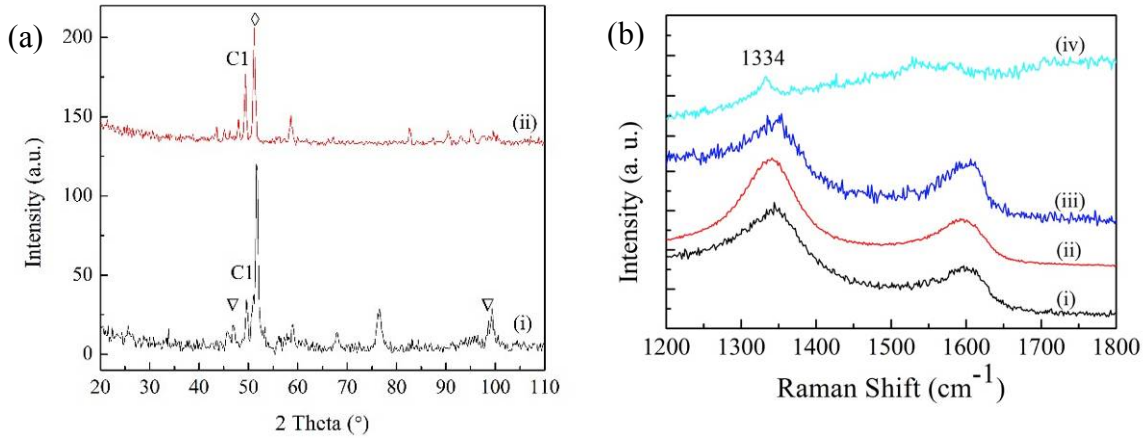
Figure 4-8. XRD patterns (a) of Fe-20Cr (i), Fe-40Cr (ii) after exposure to CH_4-H_2 plasma for 3 hrs (S: substrate, C1: $Cr_{23}C_6$; ◊: overlap of $Cr_{23}C_6$ and substrate; ▽: Fe_3C); Raman spectra (b) of Fe-20Cr (i), Fe-40Cr (ii), Fe-50Cr (iii), Fe-80Cr (iv) after exposure to CH_4-H_2 plasma for 3 hrs.
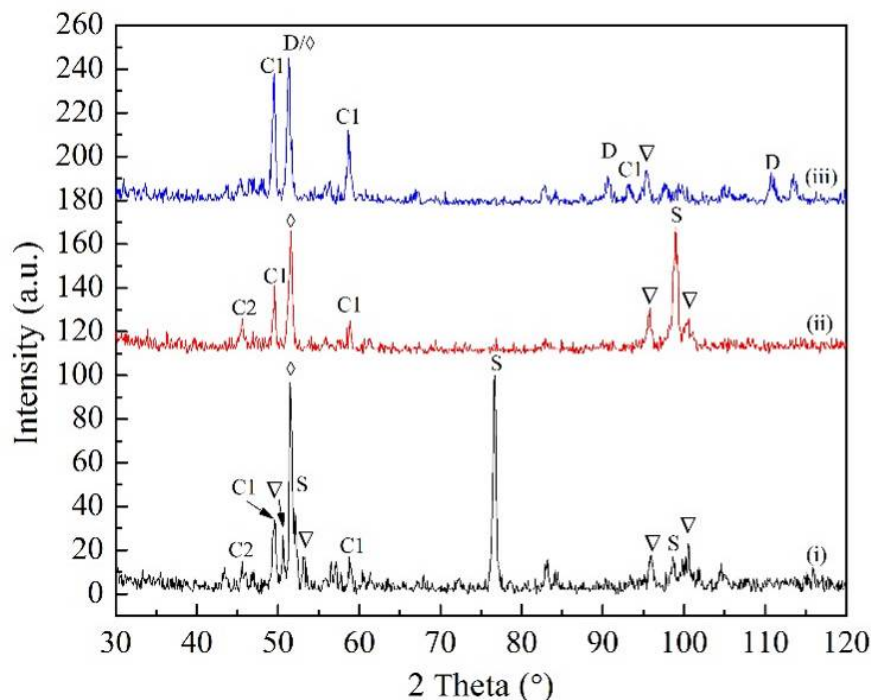
Figure 4-9. XRD patterns of Fe-20Cr (i), Fe-40Cr (ii), and Fe-80Cr (iii) after exposure to CH_4-H_2 plasma for 8 hrs. (D: diamond; C1: $Cr_{23}C_6$; C2: Cr_3C_2; S: Fe/Cr; ◊: overlap of $Cr_{23}C_6$ and substrate; ▽:Fe_3C).

The above data indicate that diamond deposition behavior is closely associated with Cr concentrations in the alloys. Previous investigations have shown that after thermal exposure in atmospheres containing CO, CO_2, hydrocarbon gases like CH_4, and C_2H_4, the conventional Cr-containing steel or heat-resisting alloys are readily susceptible to an internal carburization attack [112–118], while protective external chromia scales are difficult to develop. In a CH_4-H_2 plasma environment, the carbon activity can be described using an equilibrium reaction:

$$CH_4 = C_{abs.} + 2H_2 \qquad\qquad [4.1]$$

The released carbon may cause coke, carburization and/or metal dusting depending on the gas chemistry and substrate compositions [114,116]. In the current study, the substrates were exposed to the CH_4-H_2 plasma appropriately designed for diamond growth, in which, the gas

48

mixture was under a non-equilibrium condition, and the electron impact and collisional energy transfer would generate atomic hydrogen and various CH_x radicals like:

$$H_2 \rightarrow 2H \tag{4.2}$$

$$H + CH_4 \rightarrow CH_3 + H_2 \tag{4.3}$$

Those CHx radicals act as precursors for diamond nucleation and play an important role in diamond growth. Furthermore, the atomic hydrogen in the plasma is known to preferentially etch graphitic carbon, rather than diamond. But the exact mechanism of carbon activity within the plasma atmosphere is difficult to determine and thus the alloys show different deposition behaviors from the conventional carburization attack by nonplasma processes. Based on thermodynamic perspective, under this highly reducing atmosphere, the oxides of Cr or Fe are hard to form (see Fig. 4-10), verifying the aforementioned composition analysis [119]. In contrast, both Fe and Cr are very reactive to carbon and the ingress of carbon into the alloy facilitates the formation of their carbides. For low Cr alloys, the amount of chromium carbides formed is not large enough to sufficiently block the carburization of iron and separate the substrate from the deposition atmosphere. Accordingly, graphitization cannot be effectively suppressed. For Fe-80Cr substrate, an exclusive Cr carbide layer can quickly form due to the extremely high concentration of Cr and its higher reactivity with carbon compared to Fe. This in-situ formed Cr carbide buffer layer can effectively inhibit the formation of graphite and enhance diamond nucleation.
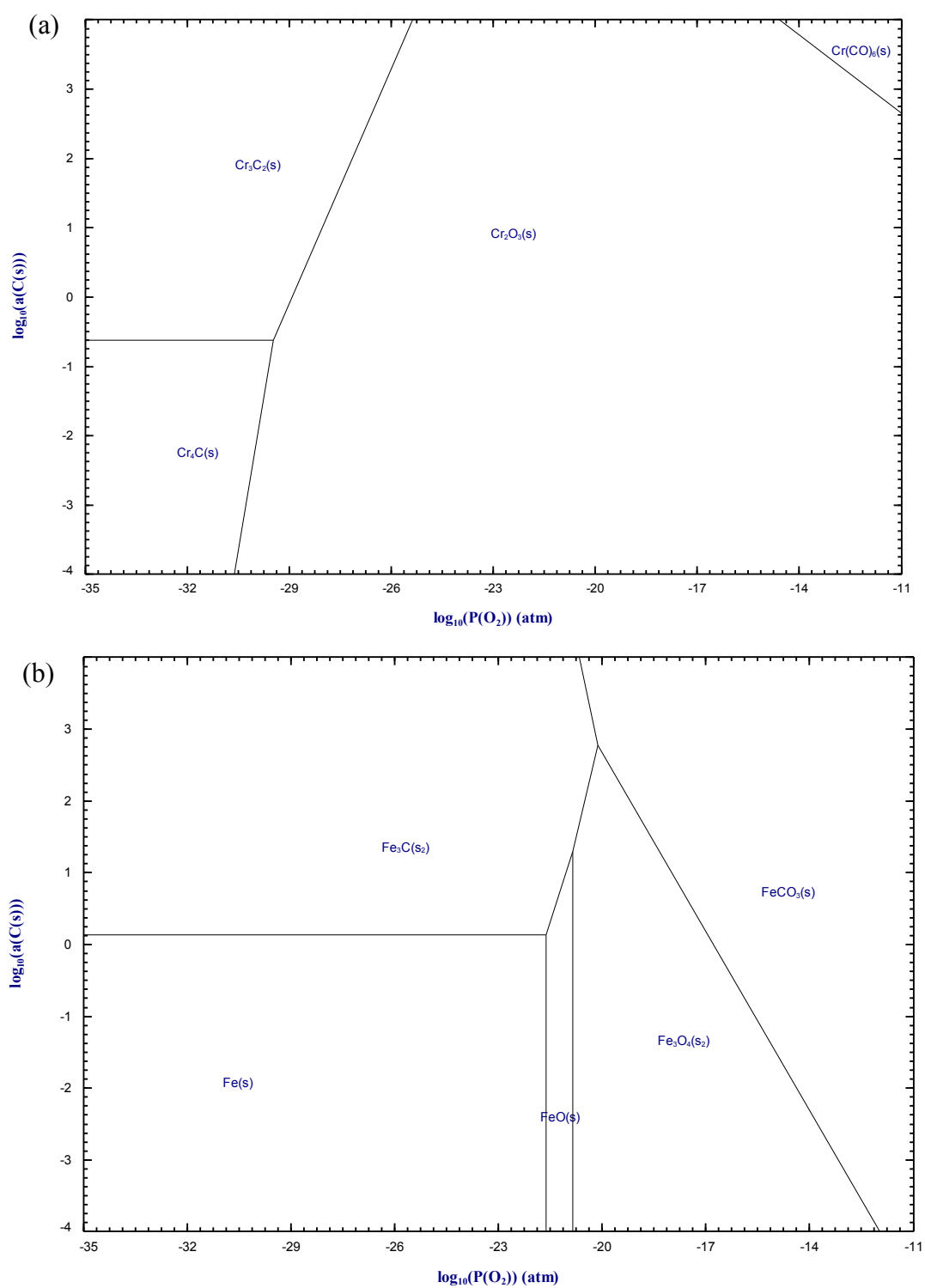
Figure 4-10. Metastable Cr-C-O (a) and Fe-C-O (b) phase diagrams at 700°C [119].

4.2　Diamond Deposition on Fe Based Substrates with Al and Al/AlN Interlayers

4.2.1　Characterization of AlN Interlayer

Figure 4-11 shows the N and Al K-edge XANES spectra of as-synthesized AlN interlayer. There is only one single peak for N, which is different from a previous report [73]. This difference is probably resulted from different preparation conditions that produce different electronic structure and chemical bonding in the AlN film. The Al K-edge spectrum shows a continuous shape consisting of several overlapped features without clear peak positions. These features indicate a superposition from different characteristic peaks of wurtzite phase (h-AlN), zincblend phase (c-AlN) and metallic Al depending on the chemical stoichiometry of the film. As interlayers play important role on diamond nucleation and adhesion, the structural information of the interlayers and its effect on diamond nucleation and adhesion is important. In order to have an in-depth understanding of the nucleation and adhesion behavior of diamond on AlN interlayered Fe based materials, the intrinsic properties of such interlayers and their effect on diamond nucleation and growth is being systematically carried on and will be reported in the near future.
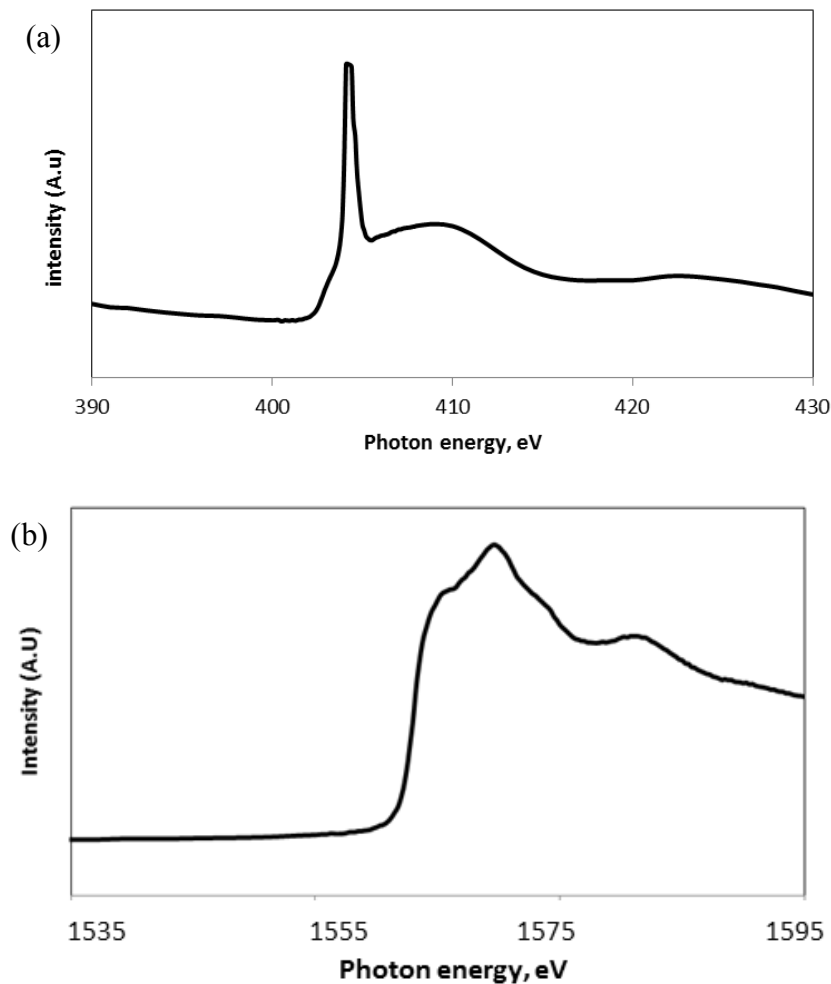
Figure 4-11. Soft x-ray absorption spectra of N (a) and Al (b) K-edge in AlN interlayer.

4.2.2 Diamond Nucleation and Growth

Figure 4-12 shows typical SEM morphologies of the diamond coatings. Diamond on Al coated SS316 (a) has the largest grain size than diamond on Al/AlN coated SS316 (b), Al coated Kovar (c), and Al/AlN coated Kovar (d). The film is porous and non-uniform. The nucleation density of diamond is higher on Al/AlN coated SS316 (b) compared to Al coated SS316 (a). After 6 hrs deposition, the coating is mostly continuous and the diamond crystals are highly oriented. On the Al coated Kovar (c), the coating is continuous and highly oriented with cube (100) faces. The crystalline structure of diamond becomes featureless on Al/AlN coated Kovar

(d) because of the fine grains. Dense and continuous diamond coatings are observed on both Al and Al/AlN coated Kovar substrates. The nucleation density of diamond is higher on Al/AlN than single Al coated ones. Fig. 4-12e and Fig. 4-12f are the low magnification images of diamond on Al and Al/AlN coated Kovar substrates, respectively. It can be seen that diamond coating on Al coated Kovar is uniform without spallation. However, on Al/AlN coated Kovar (see Fig. 4-12f), some clusters and linear defects are observed as dark sites, which might be caused by the failure of the interlayer during the pre-scratch treatment. Although crystalline AlN has higher hardness than Al, as shown in Fig. 4-11 the structure of the AlN interlayer in the present research is different from the crystalline AlN so that the AlN interlayer might not be strong enough to resist scratch treatment and has been removed partially during the scratch treatment. For both substrates, Al/AlN dual layers improve the nucleation density of diamond compared to Al monolayer. With higher diamond nucleation density, less graphite can be formed at the interface and the diamond deposited has high contact area with the substrate, thereby diamond has higher adhesion to the substrate.

The original Raman spectra of the samples are presented in Fig. 4-13 (left). Because of the huge background, the features of carbon peaks are small in original spectra. In order to make the characteristic peaks clearly show, the fluorescence background in the spectra is removed and the spectra after background removal are normalized to the diamond peaks and shown in Fig. 4-13 (right). In the spectrum of diamond deposited on Al coated SS316 (see Fig. 4-13a), a peak located at 1332.3 cm^{-1}, corresponding to natural diamond peak, and a broad peak at 1580 cm^{-1} are observed, which indicates the existence of both diamond and graphitic phase. As the Raman scattering cross-section area of graphitic phase is 50 times higher than that of diamond, the amount of graphitic phase detected in this spectrum is ignorable. Similarly, the peak at 1332.3

cm^{-1} is observed in spectrum of diamond on Al/AlN coated SS316 (Fig. 4-13b). The fact that the characteristic peak of diamond on SS316 is close to natural diamond peak without significant shift indicates that the coatings are thermal stress free. This is probably because of the spontaneous spallation of diamond coatings due to the poor adhesion. The peaks of non-diamond carbon are not shown in this spectrum, indicating high purity diamond in the coating. These results show that the addition AlN interlayer on SS316 enhances diamond formation. In the spectrum of diamond deposited on Al coated Kovar (Fig. 4-13c), a sharp peak locates at 1336.9 cm^{-1} and two broad peaks centered at 1130 cm^{-1} and 1440 cm^{-1}, probably from transpolyacetylene, and an amorphous sp^{3} carbon peak at 1220 cm^{-1} [7,67,91] are observed, whereas in the spectrum of diamond deposited on Al/AlN coated Kovar, the diamond peak is located at 1335.4 cm^{-1}, relatively closer to the natural diamond peak and the broad peak at 1130 cm^{-1} is much weaker with no peak for amorphous carbon. The diamond peaks shown in Fig. 4-13 are further fitted using Gaussian function and the full widths at half maximum (FWHM) of the fitted peaks are 11.89 cm^{-1} (a), 11.03 cm^{-1} (b), 9.29 cm^{-1} (c), 8.24 cm^{-1} (d), respectively. On Kovar substrates, the addition of AlN interlayer increases the purity of diamond coating and decreases the upward shifting of diamond peak from natural diamond peak. The upshifting of diamond peak is related to the compressive stress induced by the mismatch of thermal expansion coefficients of diamond and Kovar. The existence of compressive stresses in diamond indicates that the diamond coating adheres to the substrate without spallation. The decreased shifting suggests less stress inside the coating, indicating the addition of AlN interlayer could decrease the stress inside diamond coating on Kovar.
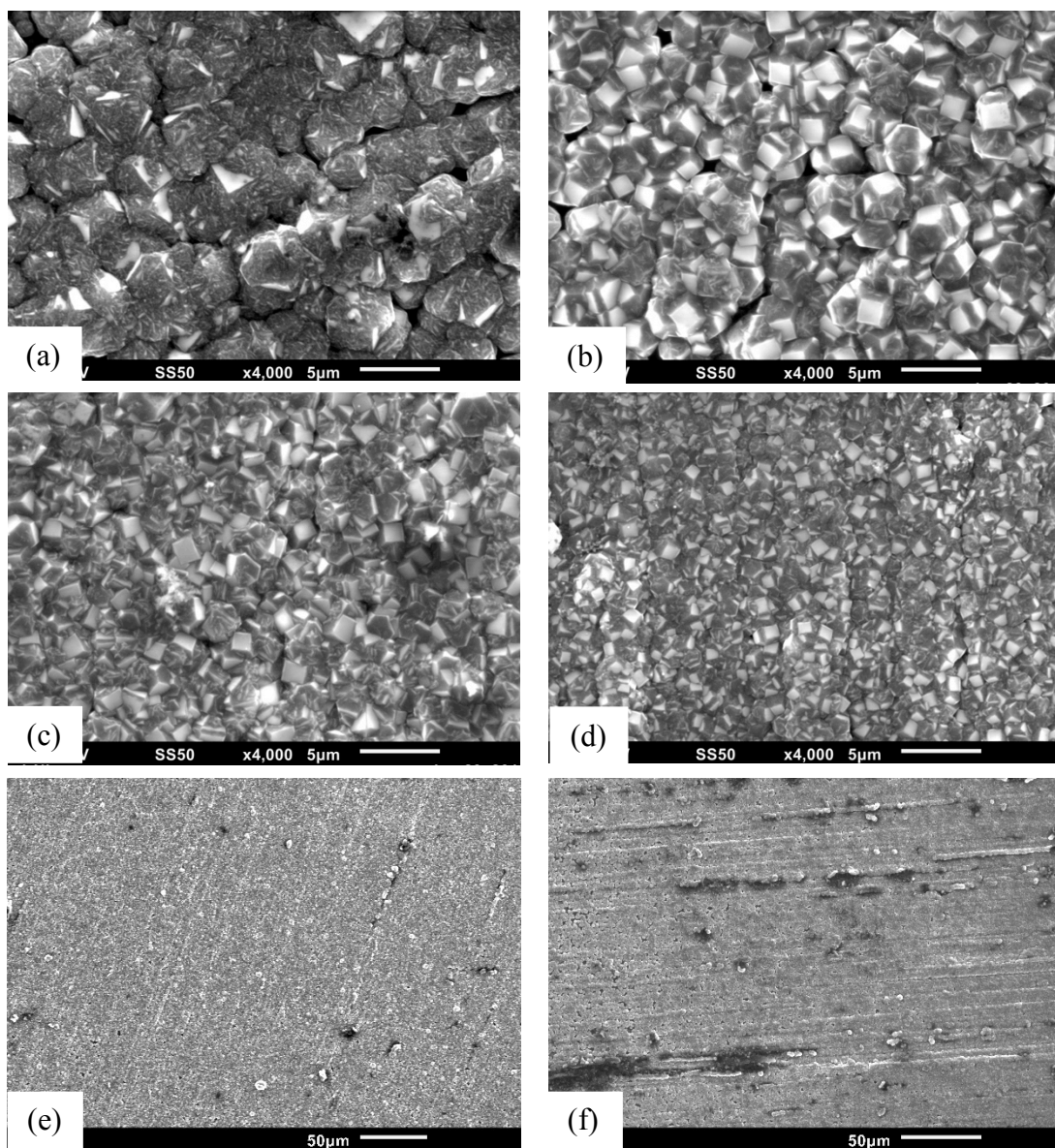
Figure 4-12. SEM images of diamond on Al coated SS316 (a), Al/AlN coated SS316 (b), Al coated Kovar (c, e), and Al/AlN coated Kovar (d, f).
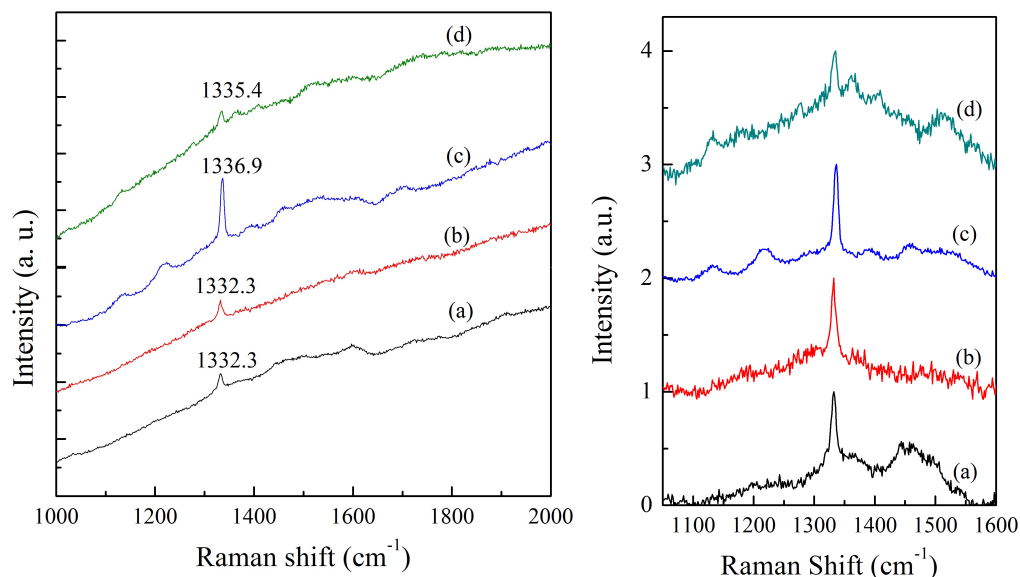
Figure 4-13. Raman spectra (left) of diamond coatings on Al coated SS316 (a), Al/AlN coated SS316 (b), Al coated Kovar (c), and Al/AlN coated Kovar (d); the corresponding Raman spectra (right) after normalization to diamond peak and background removal.

4.2.3 Interfacial Analysis

The original Raman spectra of the exposed surfaces after removing deposited diamond coating are presented in Fig. 4-14 (left). Spectrum (a) was taken on the surface after spontaneous spallation of diamond coating on Al/AlN coated SS316 while Spectrum (b) and (c) were taken on the exposed surfaces after the diamond coatings were mechanically removed from the Kovar substrates. There are two broad bands located at approximately 1355 cm^{-1} and 1600 cm^{-1}, characteristic peaks of graphite phase, appeared in all the spectra. The intensity of the peaks is very low with respect to the high background, indicating that all the interlayers are able to suppress the formation of graphite. In order to make the Raman bands clearly seen, fluorescence background of the spectra were removed and shown in the Fig. 4-14 (right). As can be seen, the intensity graphite bands in spectrum (b) are higher than that in spectra (a) and (c), indicating that the Al/AlN dual layers have better barrier effect than Al monolayer.

56
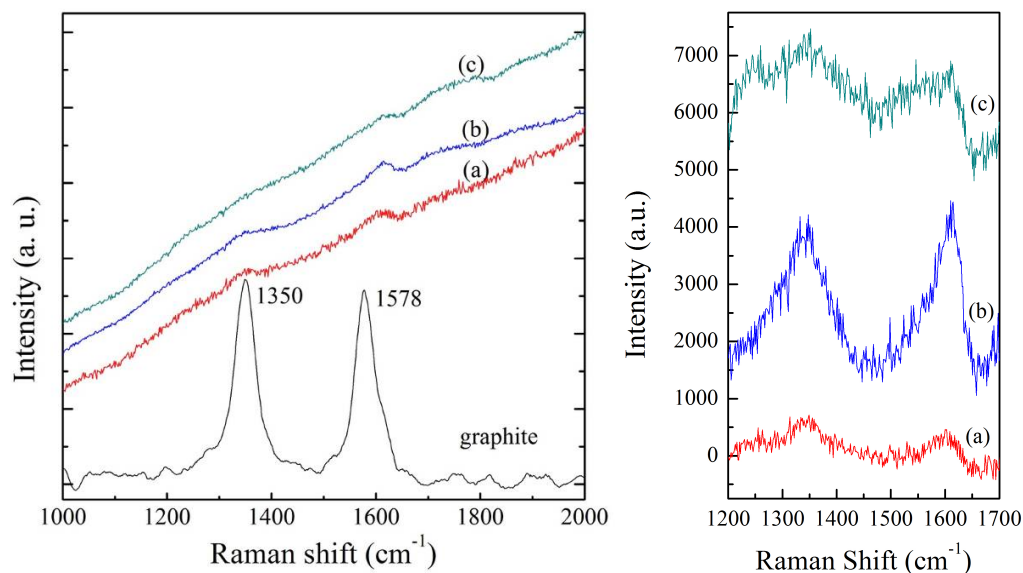
Figure 4-14. Raman spectra (left) of as-exposed surfaces after partially spallation of diamond coating on Al/AlN coated SS316 (a), Al coated Kovar (b), Al/AlN coated Kovar (c); the corresponding Raman spectra (right) after background removal.

Figure 4-15 shows the XRD patterns on Al coated Kovar (a) and Al/AlN coated Kovar (b) after diamond deposition for 6 hrs. In order to use XRD to characterize the phase changes of the substrates after diamond deposition, two Kovar samples with thinner interlayers were prepared for diamond deposition, in which the deposition time for Al monolayer was 1hr and 0.5 hr (Al), 0.5 hr (AlN) for Al/AlN multilayers. As the interlayers are ultrathin, the diffraction peaks of Al and AlN are too weak to be seen and the diffraction peaks from Kovar substrates (FeNi) can be clearly shown in both cases. After diamond deposition in CH_4-H_2 plasma, diamond peaks are too weak to be shown on Al coated Kovar whereas a weak diamond peak (111) is observed on Al/AlN coated Kovar. In addition, there are no peaks of iron carbide shown in both patterns, indicating that both Al monolayer and Al/AlN dual layers can effectively suppress carbon diffusion into Kovar, as carbon has high solubility in iron-based materials and can easily react with Fe to form carbides if carbon could diffuse into Fe based substrates.

57
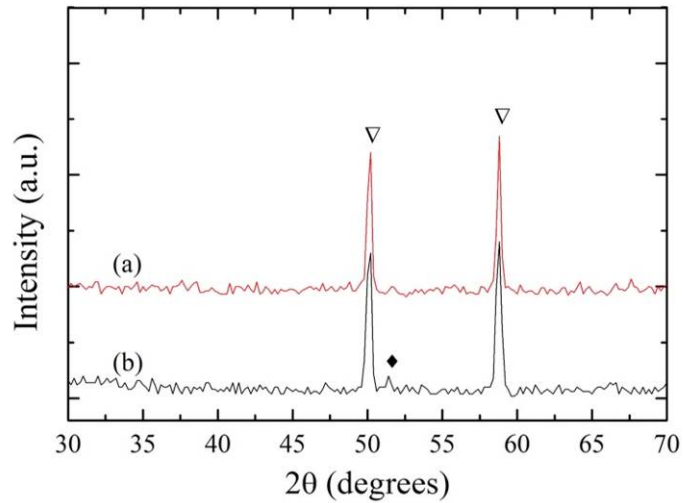
Figure 4-15. XRD patterns of Al coated Kovar (a), and Al/AlN coated Kovar (b) after 6 hrs diamond deposition ($\triangledown$: iron nickel; $\blacklozenge$: diamond).

4.2.4   Adhesion Evaluation

As shown in Figure 4-16a, severe delamination of diamond coating is observed on Al/AlN coated SS316. Because of the higher nucleation density, diamond deposited on Al/AlN coated SS316 are continuous coatings and in this case, high thermal stress would be induced by cooling from deposition temperature to room temperature because of the thermal expansion mismatch. And the high stress might result in cracks or delamination. After the spontaneous delamination, the residual stresses would be released. This release of stresses is consistent with the Raman spectra shown in Fig. 4-13a and b, where the diamond characteristic peaks are close to 1332 cm^{-1}. Unlike on SS316 substrates, well adherent diamond coatings have been obtained on Kovar substrates with either single Al interlayer or Al/AlN dual interlayers. As shown in Fig. 4-16b, only partial delamination is observed around the imprint after a high load of 1470 N was applied to the diamond coating on Al coated Kovar. These results show that diamond has a higher adhesion on Kovar substrates.
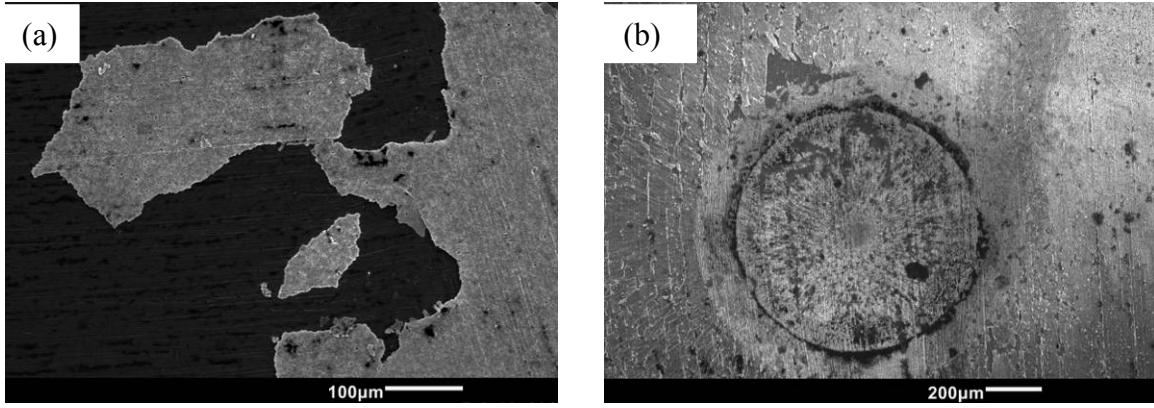
Figure 4-16. SEM images of diamond coating on Al/AlN coated SS316 after spontaneous spallation (a), and the imprint of diamond coating on Al coated Kovar after Rockwell C indentation testing (b).

The better adhesion of diamond coatings on Kovar substrates is mainly attributed to the lower thermal stress. The thermal stress between the films and substrates can be estimated from the equation:

$$\sigma_{thermal} = \frac{E}{1-\nu}\int_{20}^{T}(\alpha_f - \alpha_s)dT \qquad [4.4]$$

where E is Young's modulus of diamond (~1050 GPa); ν is the Poisson ratio of the diamond (~0.07); α_f and α_s are the thermal-expansion coefficients of the diamond film and substrate, respectively; and dT is the deposition temperature (~ 70 °C) minus room temperature [69]. The thermal expansion coefficients and the estimate thermal stresses between diamond films and different materials are shown in table 4-2. The thermal stress of diamond directly on SS316 (10.6 GPa) is much higher than on Kovar (2.9 GPa). Even the same interlayers are applied, the adhesion of diamond on SS316 and Kovar are significantly different. In this case, the thermal stress of diamond coating is more dependent on the substrate materials than the interlayer materials. The lower thermal expansion coefficient of Kovar guarantees better adhesion of diamond coatings.

Table 4-2. Estimated thermal stresses of diamond films on various materials

Materials	α (×10^{-6} K^{-1})			Thermal stress σ (GPa)
	25°C	670°C	Average	
Diamond	~0.8	~4.2	~2.5	-
Kovar	~5.0	~7.8	~6.4	2.9
SS316	~15.9	~18	~17.0	10.6
AlN	~4.8	~5.6	~5.2	2.0
Al	~23.1	~33.8	~28.45	19.0

α is the linear thermal expansion coefficients (data from "Thermal Properties of Materials", Materials Science and Engineering Handbook, CRC Press LLC, 2001, and "Thermal expansion of AlN, sapphire, and silicon", Yim, W. M. and Paff, R. J.)

Without spallation on Kovar, compressive stresses were accumulated in the diamond coatings. The upward shifted diamond peaks shown in Fig. 4-13c and d reveal these residual stress. As intermediate layers are applied on Kovar, the thermal stresses of diamond coatings are slightly modified. According to Ager et al. and Ralchenko et al. [69,70], the compressive stress can be estimated by the equation:

$$\sigma(GPa) = -0.567(v_{measured} - v_0)(cm^{-1}) \qquad [4.5]$$

where $v_{measured}$ is the center of the diamond peak measured in Raman spectrum, v_0 is the position of natural diamond peak at 1332 cm^{-1}. The calculated compressive stresses are 2.8 GPa on Al monolayer and 1.9 GPa on Al/AlN dual layers, respectively. The stress 2.8 GPa is close to the estimated stress of diamond directly on Kovar (2.9 GPa), which indicates that the Al interlayer does not affect the thermal stress between diamond and Kovar. This is probably because Al diffuses into the substrates and forms an Al rich zone like ion beam implantation of Al [13]. This thin Al rich layer might not significantly change the thermal property of the substrate. And the measured stress 1.9 GPa is close to the estimated stress of diamond directly on AlN (2.0 GPa). This is probably because ceramic AlN layer is stable and has an intermediate thermal expansion coefficient between diamond and Kovar and therefore is able to reduce the thermal stress.

Consequently, the Al/AlN dual layers could increase the adhesion of diamond coating on Kovar substrate compared to the monolayer.

Chapter 5
SUMMARY, CONCLUSIONS AND FUTURE WORK

5.1   Summary and Conclusions

In this work, diamond deposition on various Fe based substrates with and without interlayers was conducted in a MPCVD reactor. The substrate material investigated includes Fe-Cr alloys and commercial available stainless steel 316, and Kovar. Fe-Cr alloys were prepared by vacuum arc-melting and Al and AlN interlayers were synthesized by ion beam sputtering in a BTIBD system. The deposited samples and structural changes of substrate materials were characterized by various techniques, including optical microscopy, SEM, TEM, EDS, Raman spectroscopy, XANES, XRD and Rockwell C indentation test. The results summarized and concluded as follows.

1.   Fe-Cr alloy substrates with low Cr content ($\leq 50\%$) are internally carburized and voluminous graphitic carbon deposits are formed on their surfaces, along with low density diamonds grown on the graphite layer.

2.   For the Fe-80Cr substrate, the carburization of iron was suppressed and the formation of graphite was absent due to the rapid formation of an exclusively Cr carbide layer. Accordingly, the nucleation and growth of diamond on the Fe-80Cr substrate was significantly enhanced.

3.   Continuous diamond coatings were deposited on SS316 and Kovar with Al and Al/AlN interlayers. Diamond coatings show better adhesion on Kovar than on SS316, which indicates that lowering thermal expansion coefficient of the substrates can enhance the adhesion of diamond coatings.

4.   The Al and Al/AlN interlayers are effective barriers to suppress the formation of graphite at the interface and have inhibited carbon diffusion into substrate and thus no substrate carburization has been observed.

5.   The Al/AlN dual layers can enhance the nucleation and growth of diamond on Fe based substrates compared to Al monolayer. In addition, Al/AlN dual layers could reduce the thermal stress of the diamond coatings and thus enhance diamond adhesion. Consequently, well adherent diamond coatings have been deposited on Kovar substrate. However, due to the high thermal expansion coefficients of SS316, spontaneous spallation of diamond coatings has been observed on them, indicating that Kovar is a better substrate material for diamond deposition.

5.2   Recommendation for Future Work

Based on this work, I would recommend following work to be done in the future:

1.   A comprehensive interfacial analysis is needed for diamond coating on Fe-80Cr alloy in order to understand the growth mechanism. Related information on the thickness, chemical composition, fine structure, and spatial distribution of the carbide layer would be very helpful to verify the proposed assumptions and to clarify the in-depth mechanism.

2.   The effect of structure and thickness of Al and Al/AlN interlayers on diamond nucleation and adhesion needed to be investigated systematically and optimized for best adhesion. For example, the thickness and crystalline state of AlN layer would affect the residual stress of diamond coating on SS316 significantly; optimized thickness and structure for diamond nucleation and adhesion are desirable for applications.

3.   The interlayers prepared by different deposition methods would affect the structure of the layers and different diamond deposition methods might affect diamond

nucleation. It is suggested that optional techniques such as magnetron sputtering and evaporation being used to fabricate interlayers and optional method HFCVD being used to deposit diamond.

4. Multilayered immediate layers might be more effective. It is suggested that Mo, Ti, CrN combine Al/AlN being investigated.

5. Diamond deposition conditions have significant effect on diamond nucleation and adhesion. The effect of microwave power, gas composition, gas pressure, and gas flow rate are suggested to be investigated.

LIST OF REFERENCES

[1]   J.J. Gracio, Q.H. Fan, J.C. Madaleno, Diamond growth by chemical vapour deposition, J. Phys. D. Appl. Phys. 43 (2010) 374017.

[2]   A.G. Darrin, R. Osiander, MEMS Packaging Materials, in: R. Ghodssi, P. Lin (Eds.), MEMS Materials and Processes Handbook, Springer US, Boston, MA, 2011: pp. 879–923.

[3]   M. Zink, Biocompatibility of Thin Films, in: S. Nazarpour (Ed.), Thin Films and Coatings in Biology, Springer Netherlands, Dordrecht, 2013: pp. 11–67.

[4]   R. Davis, Diamond properties and applications, in: Diamond Films and Coatings, William Andrew Publishing/Noyes, Park Ridge, N.J., 1993: pp. 1–28.

[5]   M. Sivakumar, U.K. Mudali, S. Rajeswari, Compatibility of ferritic and duplex stainless steels as implant materials: in vitro corrosion performance, J. Mater. Sci. 28 (1993) 6081–6086.

[6]   R.K. Singh, D.R. Gilbert, J. Fitz-Gerald, S. Harkness, D.G. Lee, Engineered interfaces for adherent diamond coatings on large thermal-expansion coefficient mismatched substrates, Science. 272 (1996) 396–398.

[7]   W.A. Yarbrough, R. Messier, Current issues and problems in the chemical vapor deposition of diamond., Science. 247 (1990) 688–696.

[8]   L. Wang, J. Lu, Q. Su, N. Wu, J. Liu, W. Shi, Y. Xia, [100]-Textured Growth of Polycrystalline Diamond Films on Alumina Substrates By Microwave Plasma Chemical Vapor Deposition, Mater. Lett. 60 (2006) 2390–2394.

[9]   G.S. Ristić, Ž.D. Bogdanov, S. Zec, N. Romčević, Z. Dohčević-Mitrović, Š.S. Miljanić, Effect of the substrate material on diamond CVD coating properties, Mater. Chem. Phys. 80 (2003) 529–536.

[10]   N.G. Shang, Z.F. Zhou, C.S. Lee, I. Bello, S.T. Lee, Effect of ion beam nitriding on diamond nucleation and growth onto steel substrates, Diam. Relat. Mater. 10 (2001) 1506–1510.

[11]   J. Ballinger, S. a. Catledge, Metal-boride interlayers for chemical vapor deposited nanostructured NSD films on 316 and 440C stainless steel, Surf. Coatings Technol. 261 (2015) 244–252.

[12]   Y.S. Li, Q. Yang, C. Xiao, A. Hirose, Effect of various alloying elements on diamond growth on Fe–Cr steels, Thin Solid Films. 516 (2008) 3089–3093.

[13] Y.S. Li, H.T. Ma, L.Z. Yang, Q. Yang, A. Hirose, Enhanced diamond CVD synthesis on steel substrates modified by ion beam implantation and sputtering of Al, Surf. Coatings Technol. 207 (2012) 328–333.

[14] Y. Tang, Y.S. Li, C. Zhang, L. Zhang, L. Yang, Q. Yang, A. Hirose, Study of nanocrystalline diamond synthesis in MPCVD by bias enhanced nucleation and growth, Diam. Relat. Mater. 25 (2012) 87–91.

[15] E. Garratt, S. AlFaify, T. Yoshitake, Y. Katamune, M. Bowden, M. Nandasiri, M. Ghantasala, D.C. Mancini, S. Thevuthasan, a. Kayani, Effect of chromium underlayer on the properties of nano-crystalline diamond films, Appl. Phys. Lett. 102 (2013) 011913.

[16] R. Polini, F.P. Mantini, M. Braic, M. Amar, W. Ahmed, H. Taylor, Effects of Ti- and Zr-based interlayer coatings on the hot filament chemical vapour deposition of diamond on high speed steel, Thin Solid Films. 494 (2006) 116–122.

[17] Y.S. Li, Y. Tang, Q. Yang, C. Xiao, A. Hirose, Diamond deposition on steel substrates with an Al interlayer, Int. J. Refract. Met. Hard Mater. 27 (2009) 417–420.

[18] H. Wako, T. Abe, T. Takagi, T. Ikohagi, Comparison of diamond film adhesion on molybdenum substrates with different surface morphologies, Appl. Surf. Sci. 256 (2009) 1466–1471.

[19] J.G. Buijnsters, P. Shankar, W. Fleischer, W.J.P. van Enckevort, J.J. Schermer, J.J. ter Meulen, CVD diamond deposition on steel using arc-plated chromium nitride interlayers, Diam. Relat. Mater. 11 (2002) 536–544.

[20] V. Godbole, J. Narayan, Aluminum nitride buffer layer for diamond film growth, J. Mater. Res. 11 (1996) 1810–1818.

[21] Y.S. Li, Y. Tang, Q. Yang, J. Maley, R. Sammynaiken, T. Regier, C. Xiao, A. Hirose, Ultrathin W-Al dual interlayer approach to depositing smooth and adherent nanocrystalline diamond films on stainless steel, ACS Appl. Mater. Interfaces. 2 (2010) 335–338.

[22] H. Zhang, Y. Jiang, S. Yang, Z. Lin, K. Feng, Diamond growth on steel substrates with AL–N interlayer produced by high power plasma streams, Thin Solid Films. 349 (1999) 162–164.

[23] X.J. Li, L.L. He, Y.S. Li, Q. Yang, A. Hirose, Direct coating adherent diamond films on Fe-based alloy substrate: The roles of Al, Cr in enhancing interfacial adhesion and promoting diamond growth, ACS Appl. Mater. Interfaces. 5 (2013) 7370–7378.

[24] Q.H. Fan, J. Grácio, E. Pereira, N. Ali, W. Ahmed, Study of diamond adhesion behavior on chromium and titanium for obtaining adherent diamond coatings on steel, J. Mater. Res. 15 (2000) 2330–2335.

[25] C. Bareiβ, M. Perle, S.M. Rosiwal, R.F. Singer, Diamond coating of steel at high temperatures in hot filament chemical vapour deposition (HFCVD) employing chromium interlayers, Diam. Relat. Mater. 15 (2006) 754–760.

[26] X. Xiao, B.W. Sheldon, E. Konca, L.C. Lev, M.J. Lukitsch, The failure mechanism of chromium as the interlayer to enhance the adhesion of nanocrystalline diamond coatings on cemented carbide, Diam. Relat. Mater. 18 (2009) 1114–1117.

[27] Z. Khalaj, M. Ghoranneviss, E. Vaghri, O. Ponta, Diamond and Diamond-Like Carbon, in: M.V. Diudea, C.L. Nagy (Eds.), Diamond and Related Nanostructures, Springer Netherlands, Dordrecht, 2013: pp. 29–47.

[28] S.T. Lee, Z. Lin, X. Jiang, CVD diamond films: nucleation and growth, Mater. Sci. Eng. R. 25 (1999) 123–154.

[29] R.M. Nor, S.A. Bakar, T.M. Thandavan, M. Rusop, Diamond: Synthesis, Characterisation and Applications, in: N. Yahya (Ed.), Carbon and Oxide Nanostructures: Synthesis, Characterisation and Applications, Springer Berlin Heidelberg, 2011: pp. 195–217.

[30] A. Grill, Diamond-like carbon: state of the art, Diam. Relat. Mater. 8 (1999) 428–434.

[31] N. S.Goroff, Mechanism of fullerene formation, Acc. Chem. Res. (1996) 77–83.

[32] W.Z. Li, S.S. Xie, L.X. Qian, B.H. Chang, B.S. Zou, W.Y. Zhou, R.A. Zhao, G. Wang, Large-scale synthesis of aligned carbon nanotubes, Science. 274 (1996) 1701–1703.

[33] S. Fan, Self-oriented regular arrays of carbon nanotubes and their field emission properties, Science. 283 (1999) 512–514.

[34] A.K. Geim, Graphene: status and prospects, Science. 324 (2009) 1530–1534.

[35] H.O. Pierson, Handbook of carbon, graphite, diamond and fullerenes: Properties, Processing, and Applications, Noyes Publ. (1993) 1–399.

[36] Q. Yang, S. Yang, C. Xiao, A. Hirose, Transformation of carbon nanotubes to diamond in microwave hydrogen plasma, Mater. Lett. 61 (2007) 2208–2211.

[37] Q. Yang, W. Chen, C. Xiao, A. Hirose, R. Sammynaiken, Simultaneous growth of well-aligned diamond and graphitic carbon nanostructures through graphite etching, Diam. Relat. Mater. 14 (2005) 1683–1687.

[38] Q. Yang, T. Hamilton, C. Xiao, A. Hirose, A. Moewes, Plasma-enhanced synthesis of diamond nanocone films, Thin Solid Films. 494 (2006) 110–115.

[39] Q. Yang, C. Xiao, W. Chen, A. Hirose, Selective growth of diamond and carbon nanostructures by hot filament chemical vapor deposition, Diam. Relat. Mater. 13 (2004) 433–437.

[40] P.W. May, Diamond thin films: a 21st-century material, Philos. Trans. R. Soc. A. 358 (2000) 473–495.

[41] V.F. Neto, R. Vaz, M.S. a Oliveira, J. Grácio, CVD diamond-coated steel inserts for thermoplastic mould tools-Characterization and preliminary performance evaluation, J. Mater. Process. Technol. 209 (2009) 1085–1091.

[42] J.K. Park, H.J. Lee, W.S. Lee, Y.J. Baik, Effect of TiAl-based interlayer on the surface morphology and adhesion of nanocrystalline diamond film deposited on WC–Co substrate by hot filament CVD, Surf. Coatings Technol. 258 (2014) 108–113.

[43] T.C.S. Vandevelde, K. Vandierendonck, M. Van Stappen, W. Du Mong, P. Perremans, Cutting applications of DLC, hard carbon and diamond films, Surf. Coatings Technol. 113 (1999) 80–85.

[44] V. Camarchia, F. Cappelluti, G. Ghione, M.C. Rossi, P. Calvani, G. Conte, B. Pasciuto, E. Limiti, D. Dominijanni, E. Giovine, RF power performance evaluation of surface channel diamond MESFETs, Solid. State. Electron. 55 (2011) 19–24.

[45] R. Bogdanowicz, M. Sobaszek, J. Ryl, M. Gnyba, M. Ficek, Ł. Gołuński, W.J. Bock, M. Śmietana, K. Darowicki, Improved surface coverage of an optical fibre with nanocrystalline diamond by the application of dip-coating seeding, Diam. Relat. Mater. 55 (2015) 52–63.

[46] F.P. Bundy, H.T. Hall, H.M. Strong, R.H. Wentorf, Man-Made diamonds, Nature. 176 (1955) 51–55.

[47] S. Ferro, Synthesis of diamond, J. Mater. Chem. 12 (2002) 2843–2855.

[48] W. Eversole, Diamond synthesis, US Patents. (1958).

[49] B.V. Derjaguin, D. Fedoseev, V.M. Lukyanovich, B.V. Spitzin, V.A. Ryabov, A.V. Lavrentyev, Filamentary diamond crystals, J. Cryst. Growth. 2 (1968) 380–384.

[50] J.C. Angus, H.A. Will, W.S. Stanko, Growth of diamond seed crystals by vapor deposition, J. Appl. Phys. 39 (1968) 2915–2922.

[51] S. Matsumoto, Y. Sato, M. Tsutsumi, N. Setaka, Growth of diamond particles from methane-hydrogen gas, J. Mater. Sci. 17 (1982) 3106–3112.

[52] J. Karner, M. Pedrazzini, C. Hollenstein, High current d.c. arc (HCDCA) technique for diamond deposition, Diam. Relat. Mater. 5 (1996) 217–220.

[53] K.K. Chattopadhyay, S. Matsumoto, Diamond synthesis by capacitively coupled radio frequency plasma with the addition of direct current power, Appl. Phys. Lett. 67 (1995) 3972.

[54] Y. Matsui, A. Yuuki, M. Sahara, Y. Hirose, Flame structure and diamond growth mechanism of acetylene torch, Jpn. J. Appl. Phys. 28 (1989) 1718–1724.

[55] K. Kurihara, K. Sasaki, M. Kawarada, Diamond synthesis by DC plasma jet CVD, Mater. Manuf. Process. 6 (1991) 241–256.

[56] Y. Mitsuda, T. Yoshida, K. Akashi, Development of a new microwave plasma torch and its application to diamond synthesis, Rev. Sci. Instrum. 60 (1989) 249.

[57] J.J. Chang, T.D. Mantei, R. Vuppuladhadium, H.E. Jackson, Low temperature and low pressure diamond synthesis in a microwave electron cyclotron resonance discharge, Appl. Phys. Lett. 59 (1991) 1170–1172.

[58] K.E. Spear, J.P. Dismukes, Synthetic Diamond: Emerging CVD Science and Technology, John Wiley & Sons, Chichester, 1994.

[59] S.T. Lee, A nucleation site and mechanism leading to epitaxial growth of diamond films, Science. 287 (2000) 104–106.

[60] W.L. Wang, K.J. Liao, G.C. Gao, Nucleation and growth of diamond films on molybdenum, Surf. Coatings Technol. 126 (2000) 195–198.

[61] D.T. Stibbeyz, J. Tennysony, Near-threshold electron impact dissociation of H2 within the adiabatic nuclei approximation, New J. Phys. 1 (1998) 1–9.

[62] D.G. Goodwin, G.G. Gavillet, Numerical modeling of the filament-assisted diamond growth environment, J. Appl. Phys. 68 (1990) 6393–6400.

[63] M.N.R. Ashfold, P.W. May, C. a. Rego, N.M. Everitt, Thin film diamond by chemical vapour deposition methods, Chem. Soc. Rev. 23 (1994) 21–30.

[64] R.F. Egerton, Physical Principles of Electron Microscopy, Springer US, Boston, MA, 2005.

[65] J. Liu, High-Resolution Scanning Electron Microscopy, in: N. Yao, Z.L. Wang (Eds.), Handbook of Microscopy for Nanotechnology, Kluwer Academic Publishers, Boston, 2005: pp. 325–359.

[66] D. Abou-Ras, M. Nichterwitz, M.J. Romero, S.S. Schmidt, Electron Microscopy on Thin Films for Solar Cells, in: D. Abou-Ras, T. Kirchartz, U. Rau (Eds.), Advanced Characterization Techniques for Thin Film Solar Cells, Wiley, Weinheim, Germany, 2011: pp. 299–345.

[67]   D.S. Knight, W.B. White, Characterization of diamond films by Raman spectroscopy, J. Mater. Res. 4 (1989) 385–393.

[68]   J. Álvarez-Garcia, V. Izquierdo-Roca, A. Pérez-Rodriguez, Raman Spectroscopy on Thin Films for Solar Cells, in: Advanced Characterization Techniques for Thin Film Solar Cells, 2011: pp. 365–386.

[69]   J.W. Ager, M.D. Drory, Quantitative measurement of residual biaxial stress by Raman spectroscopy in diamond grown on a Ti alloy by chemical vapor deposition, Phys. Rev. B. 48 (1993) 2601–2607.

[70]   V.G. Ralchenko, a. a. Smolin, V.G. Pereverzev, E.D. Obraztsova, K.G. Korotoushenko, V.I. Konov, Y.V. Lakhotkin, E.N. Loubnin, Diamond deposition on steel with CVD tungsten intermediate layer, Diam. Relat. Mater. 4 (1995) 754–758.

[71]   C.S. Schnohr, M.C. Ridgway, Introduction to X-Ray Absorption Spectroscopy, in: C.S. Schnohr, M.C. Ridgway (Eds.), X-Ray Absorption Spectroscopy of Semiconductors, Springer Berlin Heidelberg, 2015: pp. 1–26.

[72]   P. Lagarde, P. Lagarde, Surface X-ray absorption spectroscopy: principles and some examples of applications, Ultramicroscopy. 86 (2001) 255–263.

[73]   C.W. Pao, P.D. Babu, H.M. Tsai, J.W. Chiou, S.C. Ray, S.C. Yang, F.Z. Chien, W.F. Pong, M.H. Tsai, C.W. Hsu, L.C. Chen, C.C. Chen, K.H. Chen, H.J. Lin, J.F. Lee, J.H. Guo, Electronic structures of group-III-nitride nanorods studied by x-ray absorption, x-ray emission, and Raman spectroscopy, Appl. Phys. Lett. 88 (2006) 2004–2007.

[74]   T. Mizoguchi, I. Tanaka, M. Kunisu, M. Yoshiya, H. Adachi, W.. Ching, Theoretical prediction of ELNES/XANES and chemical bondings of AlN polytypes, Micron. 34 (2003) 249–254.

[75]   M.R. Sardela, X-Ray Diffraction and Reflectivity, in: Practical Materials Characterization, 2014: pp. 1–41.

[76]   M. Ohring, Mechanical properties of thin films, in: Materials Science of Thin Films, Elsevier, 2002: pp. 711–781.

[77]   H. Kanda, K. Suzuki, O. Fukunaga, N. Setaka, Growth of polycrystalline diamond, J. Mater. Sci. 11 (1976) 2336–2338.

[78]   X. Liao, F. Lü, J. Wang, R. Yang, Direct growth of diamond films on low carbon steel, Chinese Phys. Lett. 11 (1994) 782–784.

[79]   F. Davanloo, H. Park, C.B. Collins, Protective coatings of nanophase diamond deposited directly on stainless steel substrates, J. Mater. Res. 11 (1996) 2042–2050.

[80] C.F.M. Borges, E. Pfender, J. Heberlein, Influence of nitrided and carbonitrided interlayers on enhanced nucleation of diamond on stainless steel 304, Diam. Relat. Mater. 10 (2001) 1983–1990.

[81] J.G. Buijnsters, P. Shankar, W.J.P. van Enckevort, J.J. Schermer, J.J. ter Meulen, The adhesion of hot-filament CVD diamond films on AISI type 316 austenitic stainless steel, Diam. Relat. Mater. 13 (2004) 848–857.

[82] M. Gowri, H. Li, J.J. Schermer, W.J.P. van Enckevort, J.J. ter Meulen, Direct deposition of diamond films on steel using a three-step process, Diam. Relat. Mater. 15 (2006) 498–501.

[83] M. Gowri, W.J.P. van Enckevort, J.J. Schermer, J.P. Celis, J.J. ter Meulen, J.G. Buijnsters, Growth and adhesion of hot filament chemical vapor deposited diamond coatings on surface modified high speed steel, Diam. Relat. Mater. 18 (2009) 1450–1458.

[84] J.G. Buijnsters, P. Shankar, J.J. Ter Meulen, Direct deposition of polycrystalline diamond onto steel substrates, Surf. Coatings Technol. 201 (2007) 8955–8960.

[85] S. Schwarz, S.M. Rosiwal, Y. Musayev, R.F. Singer, High temperature diffusion chromizing as a successful method for CVD-diamond coating of steel—Part II, Diam. Relat. Mater. 12 (2003) 701–706.

[86] Y.S. Li, A. Hirose, Direct coating of nanophase diamond films on steel substrate, Chem. Phys. Lett. 433 (2006) 150–153.

[87] Y.S. Li, A. Hirose, Diamond growth on Fe-Cr-Al alloy by H2-plasma enhanced graphite etching, J. Appl. Phys. 101 (2007) 073503.

[88] Y.S. Li, Y. Tang, Q. Yang, C. Xiao, A. Hirose, Al-enhanced low temperature deposition of diamond thin films on hetero-substrates, Mater. Chem. Phys. 116 (2009) 649–653.

[89] X.J. Li, L.L. He, Y.S. Li, Q. Yang, A. Hirose, TEM interfacial characterization of CVD diamond film grown on Al inter-layered steel substrate, Diam. Relat. Mater. 50 (2014) 103–109.

[90] I. Endler, A. Leonhardt, H. Scheibe, R. Born, Interlayers for diamond deposition on tool materials, Diam. Relat. Mater. 5 (1996) 299–303.

[91] Y.X. Cui, B. Shen, F.H. Sun, Influence of amorphous ceramic interlayers on tribological properties of CVD diamond films, Appl. Surf. Sci. 313 (2014) 918–925.

[92] O. Glozman, G. Halperin, I. Etsion, Study of the wear behavior and adhesion of diamond films deposited on steel substrates by use of a Cr–N interlayer, Diam. Relat. Mater. 8 (1999) 859–864.

[93] O. Glozman, A. Hoffman, Adhesion improvement of diamond films on steel subtrates using chromium nitride interlayers, Diam. Relat. Mater. 6 (1997) 796–801.

[94] L. Schäfer, M. Fryda, T. Stolley, L. Xiang, C.P. Klages, Chemical vapour deposition of polycrystalline diamond films on high-speed steel, Surf. Coatings Technol. 116-119 (1999) 447–451.

[95] A. Bohner, R. Janisch, A. Hartmaier, Ab initio investigation of diamond coatings on steel, Scr. Mater. 60 (2009) 504–507.

[96] H. Guo, Y. Qi, X. Li, Adhesion at diamond/metal interfaces: A density functional theory study, J. Appl. Phys. 107 (2010) 033722.

[97] C. Monachon, G. Schusteritsch, E. Kaxiras, L. Weber, Qualitative link between work of adhesion and thermal conductance of metal/diamond interfaces, J. Appl. Phys. 115 (2014) 123509.

[98] Q.H. Fan, A. Fernandes, E. Pereira, J. Grácio, Adhesion of diamond coatings on steel and copper with a titanium interlayer, Diam. Relat. Mater. 8 (1999) 1549–1554.

[99] F.J.G. Silva, A.P.M. Baptista, E. Pereira, V. Teixeira, Q.H. Fan, A.J.S. Fernandes, F.M. Costa, Microwave plasma chemical vapour deposition diamond nucleation on ferrous substrates with Ti and Cr interlayers, Diam. Relat. Mater. 11 (2002) 1617–1622.

[100] M. Reinoso, F. Álvarez, H. Huck, Hard carbon coatings deposited on steel, Appl. Surf. Sci. 254 (2007) 181–184.

[101] R. Haubner, B. Lux, Diamond deposition on steel substrates using intermediate layers, Int. J. Refract. Met. Hard Mater. 24 (2006) 380–386.

[102] Q. Wei, Z.M. Yu, M.N.R. Ashfold, Z. Chen, L. Wang, L. Ma, Effects of thickness and cycle parameters on fretting wear behavior of CVD diamond coatings on steel substrates, Surf. Coatings Technol. 205 (2010) 158–167.

[103] Q. Wei, Z.M. Yu, M.N.R. Ashfold, L. Ma, Z. Chen, Fretting wear and electrochemical corrosion of well-adhered CVD diamond films deposited on steel substrates with a WC–Co interlayer, Diam. Relat. Mater. 19 (2010) 1144–1152.

[104] a. Fayer, O. Glozman, A. Hoffman, Deposition of continuous and well adhering diamond films on steel, Appl. Phys. Lett. 67 (1995) 2299–2301.

[105] V.F. Neto, R. Vaz, N. Ali, M.S. a Oliveira, J. Grácio, Diamond coatings on 3D structured steel, Diam. Relat. Mater. 17 (2008) 1424–1428.

[106] K. Kellermann, C. Bareiß, S.M. Rosiwal, R.F. Singer, Well adherent diamond coatings on steel substrates, Adv. Eng. Mater. 10 (2008) 657–660.

[107] K. Kellermann, S. Ehrhardt, J. Fandrey, S.M. Rosiwal, R.F. Singer, Influence of surface roughness on the tribological properties of HF-CVD diamond coated heat-treatable steel, Wear. 269 (2010) 811–815.

[108] Y.S. Li, Y. Tang, Q. Yang, C. Xiao, A. Hirose, Growth and adhesion failure of diamond thin films deposited on stainless steel with ultra-thin dual metal interlayers, Appl. Surf. Sci. 256 (2010) 7653–7657.

[109] Y.S. Li, X.Y. Sun, L.Z. Yang, E.Z. Kurmaev, Q. Yang, CVD Diamond Coating on Al-Interlayered FeCoNi Alloy Substrate: An Interfacial Study, High Temp. Mater. Process. (2015).

[110] H.C. Shih, C.P. Sung, C.K. Lee, W.L. Fan, J.G. Chen, Application of diamond coating to tool steels, Diam. Relat. Mater. 1 (1992) 605–611.

[111] Q. Yang, C. Xiao, A. Hirose, Plasma-enhanced deposition of nano-structured carbon films, Plasma Sci. Technol. 7 (2005) 2660–2664.

[112] T. Gheno, D. Monceau, J. Zhang, D.J. Young, Carburisation of ferritic Fe-Cr alloys by low carbon activity gases, Corros. Sci. 53 (2011) 2767–2777.

[113] T. Gheno, D. Monceau, D.J. Young, Kinetics of breakaway oxidation of Fe-Cr and Fe-Cr-Ni alloys in dry and wet carbon dioxide, Corros. Sci. 77 (2013) 246–256.

[114] D.J. Young, J. Zhang, C. Geers, M. Schütze, Recent advances in understanding metal dusting: A review, Mater. Corros. 62 (2011) 7–28.

[115] D. Young, P. Huczkowski, T. Olszewski, T. Hüttel, L. Singheiser, W.J. Quadakkers, Non-steady state carburisation of martensitic 9–12%Cr steels in CO_2 rich gases at 550°C, Corros. Sci. 88 (2014) 161–169.

[116] H.J. Grabke, Thermodynamics, mechanisms and kinetics of metal dusting, Mater. Corros. 49 (1998) 303–308.

[117] A. Rouaix-Vande Put, K. a Unocic, M.P. Brady, B. a Pint, Performance of chromia- and alumina-forming Fe- and Ni-base alloys exposed to metal dusting environments: The effect of water vapor and temperature, Corros. Sci. 92 (2015) 58–68.

[118] T.D. Nguyen, J. Zhang, D.J. Young, Water vapour effects on corrosion of Fe–Cr and Fe–Cr–Ni alloys containing cerium and manganese in CO_2 gas at 818°C, Corros. Sci. 89 (2014) 220–235.

[119] C.W. Bale, P. Chartrand, S.A. Degterov, G. Eriksson, K. Hack, R. Ben Mahfoud, J. Melançon, A.D. Pelton, S. Petersen, FactSage thermochemical software and databases, Calphad. 26 (2002) 189–228.